A TRIDENT SCHOLAR PROJECT REPORT

NO. 460

Study of Doubly-Charged Delta Baryons in Collisions of Copper Nuclei at the Relativistic Heavy Ion Collider

by

Midshipman 1/C Joseph J. Simpson, USN

UNITED STATES NAVAL ACADEMY
ANNAPOLIS, MARYLAND

USNA-1531-2

REPORT DOCUMENTATION PAGE

Form Approved
OMB No. 0704-0188

1. REPORT DATE *(DD-MM-YYYY)*	**2. REPORT TYPE**	**3. DATES COVERED** *(From - To)*
05-22-17		

4. TITLE AND SUBTITLE

Study of Doubly-Charged Delta Baryons in Collisions of Copper Nuclei at the Relativistic Heavy Ion Collider

5a. CONTRACT NUMBER

5b. GRANT NUMBER

5c. PROGRAM ELEMENT NUMBER

6. AUTHOR(S)
Joseph J. Simpson

5d. PROJECT NUMBER

5e. TASK NUMBER

5f. WORK UNIT NUMBER

7. PERFORMING ORGANIZATION NAME(S) AND ADDRESS(ES)

8. PERFORMING ORGANIZATION REPORT NUMBER

9. SPONSORING / MONITORING AGENCY NAME(S) AND ADDRESS(ES)
U.S. Naval Academy
Annapolis, MD 21402

10. SPONSOR/MONITOR'S ACRONYM(S)

11. SPONSOR/MONITOR'S REPORT NUMBER(S)
Trident Scholar Report no. 460 (2017)

12. DISTRIBUTION / AVAILABILITY STATEMENT

This document has been approved for public release; its distribution is UNLIMITED.

13. SUPPLEMENTARY NOTES

14. ABSTRACT

Experiments involving heavy-ion collisions at the Relativistic Heavy Ion Collider (RHIC) produce the hottest matter known to humans, approximately 100,000 times hotter than the center of the Sun or 7 trillion degrees Celsius. In these collisions, the nucleons melt into their constituent quarks and gluons for approximately 10 yoctoseconds (1E-23 seconds). As the collision system expands and cools, the quarks and gluons combine into particles via a process called "hadronization" and subsequently stream out into the detectors. Detailed studies of these produced particles can yield information about the properties of the medium in which they were produced. Some of the produced particles, known collectively as "resonances," have lifetimes comparable to the lifetime of the collision medium itself.

In this project, we utilize data from 24.4 million collisions of copper nuclei at center-of-mass energies of 200 GeV per nucleon pair collected by the Solenoidal Tracker At RHIC (STAR) detector to reconstruct decays of the doubly-charged Delta baryon resonance and its anti-particle. Fits to the invariant mass distribution of Delta candidates are performed as functions of transverse momentum and collision centrality and properties of the Delta resonances are extracted statistically. Specifically we look at the mass, the width, and the yield of this resonance. Comparisons of our results with previous studies from proton on proton collisions and deuteron on gold nucleus collisions, as well as with model calculations, may provide deeper insight into effects present in the collision medium as well as the lifetime of the medium itself.

15. SUBJECT TERMS
Resonances, Nuclear, Physics, RHIC, Heavy-ion, QGP

16. SECURITY CLASSIFICATION OF:			**17. LIMITATION OF ABSTRACT**	**18. NUMBER OF PAGES**	**19a. NAME OF RESPONSIBLE PERSON**
a. REPORT	**b. ABSTRACT**	**c. THIS PAGE**		59	**19b. TELEPHONE NUMBER** *(include area code)*

U.S.N.A. --- Trident Scholar project report; no. 460 (2017)

STUDY OF DOUBLY-CHARGED DELTA BARYONS IN COLLISIONS OF COPPER NUCLEI AT THE RELATIVISTIC HEAVY ION COLLIDER

by

Midshipman 1/C Joseph J. Simpson
United States Naval Academy
Annapolis, Maryland

_____
(signature)

Certification of Adviser(s) Approval

Associate Professor Richard A. Witt
Physics Department

_____
(signature)

_____
(date)

Acceptance for the Trident Scholar Committee

Professor Maria J. Schroeder
Associate Director of Midshipman Research

_____
(signature)

_____
(date)

USNA-1531-2

Experiments involving heavy-ion collisions at the Relativistic Heavy Ion Collider (RHIC) produce the hottest matter known to humans, approximately 100,000 times hotter than the center of the Sun or 7 trillion degrees Celsius. In these collisions, the nucleons melt into their constituent quarks and gluons for approximately 10 yoctoseconds (1E-23 seconds). As the collision system expands and cools, the quarks and gluons combine into particles via a process called "hadronization" and subsequently stream out into the detectors. Detailed studies of these produced particles can yield information about the properties of the medium in which they were produced. Some of the produced particles, known collectively as "resonances," have lifetimes comparable to the lifetime of the collision medium itself. More specifically, comparative studies of the relative production of short-lived resonances and possible modifications of their properties by medium effects may provide information about the conditions present in and lifetime of the collision medium.

In this project, we utilize data from 24.4 million collisions of copper nuclei at center-of-mass energies of 200 GeV per nucleon pair collected by the Solenoidal Tracker At RHIC (STAR) detector to reconstruct decays of the doubly-charged Delta baryon resonance and its anti-particle. Fits to the invariant mass distribution of Delta candidates are performed as functions of transverse momentum and collision centrality and properties of the Delta resonances are extracted statistically. Specifically we look at the mass, the width, and the yield of this resonance. Comparisons of our results with previous studies from proton on proton collisions and deuteron on gold nucleus collisions, as well as with model calculations, may provide deeper insight into effects present in the collision medium as well as the lifetime of the medium itself.

KEYWORDS: Resonances, Nuclear, Physics, RHIC, Heavy-ion, QGP.

Acknowledgments

I would like to express my sincere thanks to Prof. Richard Witt, for his constant support and guidance. I am especially thankful to him for his patient replies to my many questions, as well as always having his office open. I thank the members of the USNA Physics Department who offered advice for my final presentation, particularly Prof. McIlhany. I also thank the Trident Committee, especially Prof. Schroeder, for making it possible for me to pursue this project.

We thank the RHIC Operations Group and RCF at BNL, the NERSC Center at LBNL, and the Open Science Grid consortium for providing resources and support. This work was supported in part by the Office of Nuclear Physics within the U.S. DOE Office of Science, the U.S. National Science Foundation, the Ministry of Education and Science of the Russian Federation, National Natural Science Foundation of China, Chinese Academy of Science, the Ministry of Science and Technology of China and the Chinese Ministry of Education, the National Research Foundation of Korea, GA and MSMT of the Czech Republic, Department of Atomic Energy and Department of Science and Technology of the Government of India; the National Science Centre of Poland, National Research Foundation, the Ministry of Science, Education and Sports of the Republic of Croatia, RosAtom of Russia and German Bundesministerium fur Bildung, Wissenschaft, Forschung and Technologie (BMBF) and the Helmholtz Association.

Contents

1 The Physics of Relativistic Heavy Ion Collisions **4**

1.1 Quarks and Gluons 4

1.2 Nuclear Matter Phase Diagram and Heavy Ion Collisions 7

1.2.1 Quark Gluon Plasma (QGP) 7

1.2.2 Important Aspects of Heavy Ion Collisions 9

2 RHIC and the STAR Experiment **11**

2.1 The Relativistic Heavy Ion Collider (RHIC) 11

2.2 The Solenoidal Tracker at RHIC (STAR) 13
2.2.1 The Time Projection Chamber (TPC) 14
2.2.2 Particle Identification 17

3 Delta Baryons and Statistical Analysis Methods 18
3.1 Interest in the Delta Baryon (Δ) 19
3.1.1 Δ Yield Modifications 19
3.1.2 Δ Mass and Width Modifications 21
3.2 Reconstruction and Combinatoric Background Subtraction 21
3.3 Cuts 24

4 Yield, Mass, and Width Determination for Delta Baryons 27
4.1 Relativistic Breit-Wigner Fits 27
4.2 Relativistic Breit-Wigner Mass and Width 28
4.3 Yield Determination 46
4.3.1 Acceptance and Efficiency Corrections 46
4.3.2 Transverse Momentum Spectra Fits 47

5 Conclusions 51

A Glossary of Terms 58

1 The Physics of Relativistic Heavy Ion Collisions

Many of the descriptions in this report include terms which are specific to the field of high energy nuclear physics. To assist the reader we have included a glossary of terms in the appendix. Other terms are defined within the text itself.

1.1 Quarks and Gluons

High energy nuclear physics is a field of research that studies subatomic interactions under extreme conditions. These extreme conditions are created by smashing the nuclei of atoms together in violent collisions. Within these collisions temperatures become approximately 100,000 times hotter than the center of the Sun or 7 trillion degrees Celsius. Only with such violent collisions is it possible for us to study quarks and gluons, known collectively as "partons," which are the fundamental particles that comprise ourselves and all the matter around us. The interactions between partons, via the strong nuclear force, govern matter at its most fundamental level. Partons bind together in various ways to create larger particles that we are more familiar with, such as protons and neutrons. An illustration of the relationship between an atom, its nucleus, and partons trapped within a nucleon is shown in Figure 1 [1]. Partons, as well as electrons, are classified as fundamental particles because there is no evidence that these particles have any substructure.

Partons cannot be isolated singularly due to a phenomenon known as "confinement". Explained by the theory of Quantum Chromodynamics (QCD), the strong nuclear force becomes incredibly strong as quarks are pulled apart [2]. The energy between quarks that are being pulled apart becomes so high that many new quark-antiquark pairs may be pulled from the vacuum. This is known as "fragmentation" and results in many new pairs of quarks that still cannot be separated. The amount of quarks produced by a fragmentation is dependent on the energy of the initial fragmenting quarks. Within QCD, the prefix "chromo" means color and refers to the three types of color charge that partons can have; red, blue, or green. Color charge is an internal degree of freedom and is not related to visible color. Similar to the relation between positive and negative electric charge, partons can also have anti-red, anti-blue, or anti-green color charge.

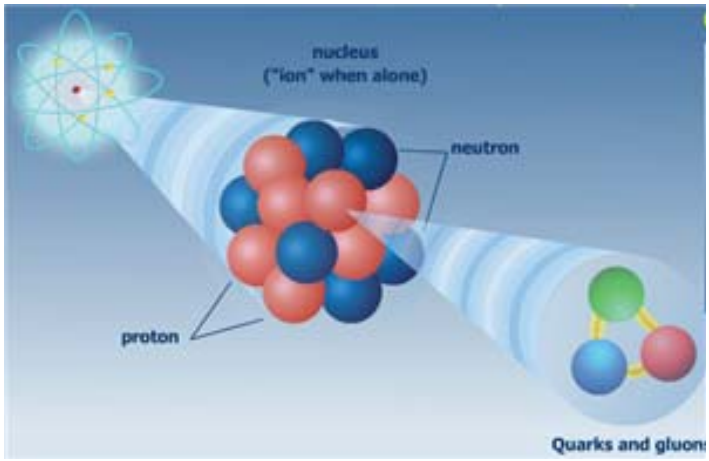

Figure 1: The top left shows Bohr's model of an atom with negatively charged electrons orbiting a positively charged dense nucleus. In the center, the nucleus is enlarged to show the protons and neutrons that it is composed of. Protons and neutrons within a nucleus are known as "nucleons." In the bottom right, there is an enlarged nucleon revealing the quarks and gluons within. There are three quarks represented by the three circles within the nucleon. There are also three gluons shown as lines connecting the three quarks.

Composite particles composed of partons are known as "hadrons" and must have a neutral color charge. There are six distinct flavors of quarks that can be bound together in various ways to create a large number of different hadrons. The six flavors of quarks, listed from lightest to heaviest, are "up," "down," "strange," "charm," "bottom," and "top." Hadrons composed of three valence quarks, each with its own color charge, are known as "baryons." Protons and neutrons are both examples of baryons. Protons are composed of two up quarks and a down quark, while neutrons are composed of two down quarks and an up quark. "Up" and "down" quarks are the lightest and most common of the different types of quarks. Up, down, and strange quarks are referred to as "light quarks," while charm, bottom, and top quarks are referred to as "heavy quarks." Heavy quarks are much less common due to the energy required to create quarks with such high mass.

Hadrons composed of a quark bound to an antiquark are known as "mesons." Pions are the most common type of mesons and consist of either an up or down quark bound to either an up or down antiquark. As mesons are composed of quark-antiquark pairs they are always able to decay by matter-antimatter annihilation. Gluons are the mediators of the strong nuclear force and "glue" quarks together within hadrons. Along with color charge, quarks also carry electric charge and are

responsible for the positive charge of protons and neutral charge of neutrons. The up quark has positive charge equivalent to two-thirds the charge of an electron, and the down quark has negative charge equivalent to one-third the charge of an electron.

The number of baryons that exist is a conserved quantity. Protons are the most common baryon because they are the lightest of all the baryons. As heavier baryons decay, lighter baryons must be produced to conserve baryon number and this ultimately leads to the production of protons. Protons are the only stable baryons with the exception being that neutrons trapped within a stable nucleus are also stable. The different baryons, composed of various combinations of quarks, will have lifetimes dependent on which fundamental force is responsible for their decay. It is unpredictable exactly how long a specific particle will take to decay so we use the mean lifetime for each group of identical particles. Baryons may decay through three of the four fundamental forces. These three forces listed in order of strongest to weakest are the strong nuclear force, the electromagnetic force, and the weak nuclear force. Baryons that decay via the strong nuclear force have the shortest mean lifetimes, while others that decay via the electromagnetic force or weak nuclear force have mean lifetimes several orders of magnitude longer.

The existence of quarks within the substructure of nucleons has been verified through deep-inelastic electron-nucleon scattering experiments. In these experiments high energy electrons are scattered off of nucleons in order to measure the internal structure of the nucleons. The confinement of quarks, as well as the phenomenon of fragmentation, is evidence that the strong nuclear force pulls partons together with incredible strength on large distance scales. Note that large distances within the nucleus may only be a few femtometers. However, the results from the deep-inelastic electron-nucleon scattering experiments showed a different result for electron-quark interactions with very large momentum transfers. The quarks within the nucleons interacting on small distance scales were able to behave almost as if they were free particles. The strong coupling of quarks on large distance scales and the relative freedom of quarks on small distance scales are two remarkable features of QCD [3].

1.2 Nuclear Matter Phase Diagram and Heavy Ion Collisions

1.2.1 Quark Gluon Plasma (QGP)

The phenomenon of confinement is a significant barrier to studying partons. Partons are always trapped within hadrons and can never be isolated singularly to be examined as independent particles. However, the results from deep-inelastic electron-nucleon scattering experiments, showing the quasi-freedom of quarks confined within nucleons, have led to an alternative method to study partons without a need for isolation. Within mediums at very high baryon densities and very high temperatures partons behave as if they are no longer confined within nucleons and "deconfinement" occurs. Mediums with sufficiently high baryon density and temperature to cause the deconfinement of partons are classified as a new phase of matter known as "Quark Gluon Plasma" (QGP).

In order to create conditions with high enough baryon density and temperature for the formation of QGP, high energy nuclear physicists use collisions between the nuclei of atoms. The bare nuclei of heavier elements, such as copper (Cu) and gold (Au), are known as "heavy ions." An ion is an atom or molecule with net electric charge, bare nuclei have a large positive charge due to the absence of electrons. Beams of heavy ions are accelerated to extreme speeds, near the speed of light, and smashed together. Such extreme speeds are required to have enough energy available within the collision medium for the formation of QGP. The nucleons involved in a collision are forced to create a medium with extremely high temperature and baryon density. If the temperature and baryon density of the medium produced by the collision become high enough, the nucleons will melt and QGP will be formed. The nuclear matter phase diagram showing the transition from hadronic matter to QGP is shown in Figure 2 [4].

The nuclear matter phase diagram shows how the phase transition from hadronic matter to QGP depends on temperature and baryon density. Hadronic matter is shown in the lower-left of the diagram at low temperature and baryon density. QGP is formed as temperature or baryon density become very large. LHC stands for Large Hadron Collider, and RHIC stands for Relativistic Heavy Ion Collider. These are the two largest machines that produce heavy ion collisions for physicists to study. Physicists using LHC and RHIC explore various regions of this diagram by varying collision

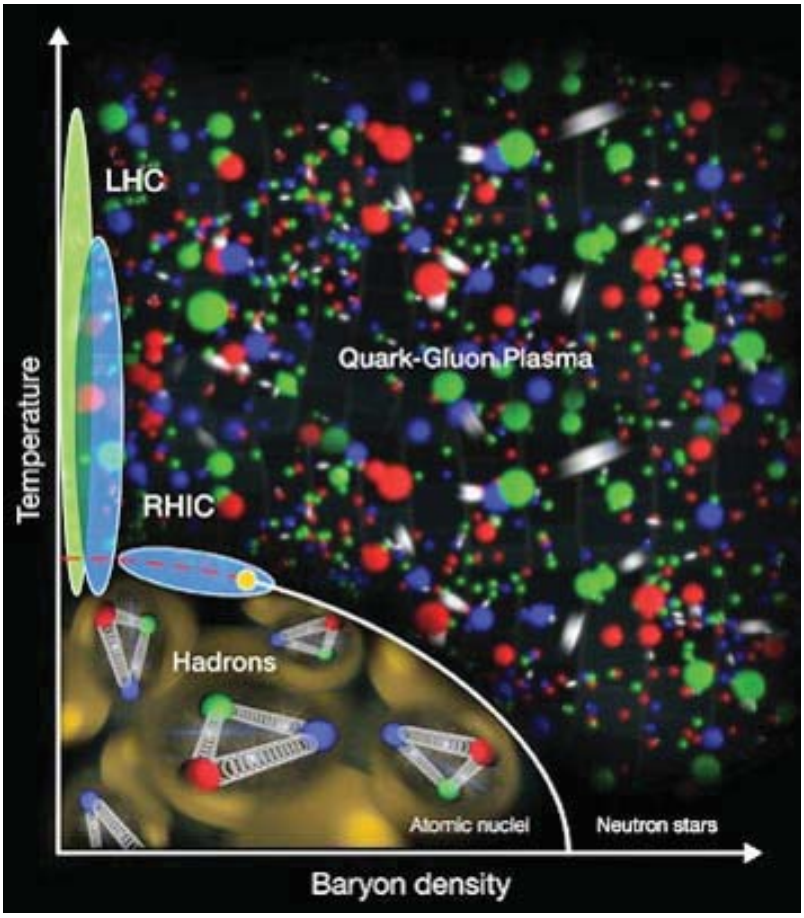

Figure 2: This is an artistic rendering of the Nuclear Matter Phase Diagram. The y-axis shows temperature and the x-axis shows baryon density.

size and energy. Neutron stars are shown in the lower-right region of the diagram. While heavy ion collisions create QGP mainly by creating very high temperatures, neutron stars create QGP by creating very high baryon densities. Neutron stars have such a powerful gravitational pull that hadrons are crushed together and QGP is formed.

Partons within a QGP will behave as free particles only if they remain within the QGP. If partons escape the QGP, or if the baryon density or temperature of the QGP are no longer high enough, they will be forced back into bound states within hadrons. This process is known as "hadronization" and returns quarks back to a condition of confinement. Two important milestones occur within a heavy ion collsion after hadronization. The first is the chemical equilibrium of the system and occurs when the resulting amounts of particles no longer change on average. This

means that the creation and annihilation of particles have reached their equilibrium values. The time at which the system reaches chemical equilibrium is known as "chemical freeze-out." The second milestone of the system occurs when the system has expanded enough that particles no longer interact. The time at which this occurs is known as "kinetic freeze-out."

The temperature sufficient to create QGP within heavy ion collisions is about 100,000 times hotter than the center of our sun (trillions of degrees Celsius). QGP is essentially an extremely hot quark gluon fire ball. In QGP, quarks enjoy a quasi-free state as they are freed from their nucleons so long as they remain in the medium. Although the protons and neutrons present within the heavy ions before the collision are made up of only two types of quarks (up and down), other types of heavier quarks form in quark-antiquark pairs within the QGP if enough energy is available. Conservation of electric charge, and color charge, is not violated by the formation of quark-antiquark pairs because these pairs will always have zero net charge. The antiquark will always have the opposite charges of the quark. For example a strange quark, with red color charge and negative one-third electric charge, will be produced with a strange antiquark that has anti-red color charge and positive one-third electric charge.

1.2.2 Important Aspects of Heavy Ion Collisions

There are many aspects of heavy ion collisions that allow us to learn about parton interactions and the formation of QGP. Three important areas of interest are collision energy, collision size, and intensity of interactions. Collision energy is determined by the design of the machine creating the collisions. Heavy ions that collide at higher speeds release more energy upon impact. A heavy ion beam being collided into stationary targets will have lower energy collisions than two heavy ion beams being collided with each other. Machines are carefully designed to achieve target energies. Machines are also designed for different collision systems, such as Cu+Cu or Au+Au. This is one way to study effects related to collision size because Au+Au collisions should be larger than Cu+Cu collisions.

Even within the same collision system every collision is unique. Some collisions will be direct

head on collisions between the heavy ions, while others will only be glancing blows. This aspect of the collisions is known as "centrality" and is related to how many nucleons participate in the collision. Studying collisions within the same collision system that have different centralites is the second way to study collision size. Baryon density is related to how many nucleons participate in each collision. Central collisions will have a higher baryon density and will be more likely to produce QGP, while peripheral collisions will have a lower baryon density and will be less likely to produce QGP. In order to understand how the size of collisions affects the formation of QGP, we must search for evidence of QGP in both central and peripheral collisions as well as collisions with centralities in between.

Figure 3 shows an illustration of a heavy ion collision [5, 6]. To do a complete study of collision size, it is necessary to compare collisions between multiple centralities and collision systems. The two heavy ions are travelling near the speed of light in opposite directions and have just collided. This collision is not directly head on and helps to illustrate how the size of the collision depends on centrality. The larger white spheres, shown at the top-right and bottom-left, represent nucleons that did not participate in the collision. These non-participant nucleons are known as "spectators" and are classified as cold nuclear matter. The nucleons that did participate in the collision, known as "participants," have been transformed into QGP. The QGP is shown in the center, stretching to the left and right, and is illustrated by the smaller red, blue, and green spheres that represent the three color charges of quarks.

To study the intensity of parton interactions within heavy ion collisions we divide the interactions into two categories, "hard-scattering" and "soft-scattering." Hard-scattering interactions are the initial parton-parton collisions that occur when the heavy ions first collide. Very high momentum partons scatter off of each other and are thrown from the medium. Once one of these high momentum partons is ejected from the medium, fragmentation occurs and a spray of hadrons is created in the direction the parton was traveling. A spray of hadrons created in this way is known as a "jet." Soft-scattering interactions are all the secondary lower momentum interactions that occur within the medium. Looking for effects dependent on the momentum of particles produced

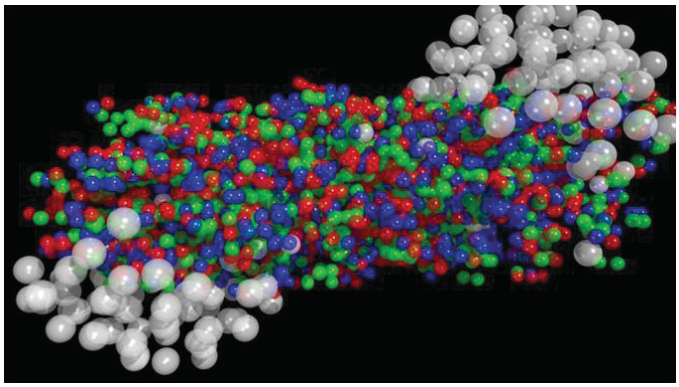

Figure 3: Shown is an illustration of a heavy ion collision. The larger white spheres, shown at the top-right and bottom-left, represent spectator nucleons. The QGP is shown in the center, stretching to the left and right, and is illustrated by the smaller red, blue, and green spheres that represent the three color charges of quarks.

by heavy ion collisions yields information about the nature of parton interactions from soft or hard-scattering.

2 RHIC and the STAR Experiment

2.1 The Relativistic Heavy Ion Collider (RHIC)

The Relativistic Heavy Ion Colleder (RHIC) was carefully built to have the ability to collide nuclei with atomic masses ranging from 1 to as high as 200 at varying energies. This allows RHIC to create collision mediums with varying temperatures and baryon densities so that physicists can carefully study QGP and the Nuclear Matter Phase Diagram. Unlike earlier particle accelerators which collided a single beam of particles into a stationary target, RHIC collides two beams of particles together in order to get much higher energy collisions. When RHIC began data collection in the year 2000, it was the first and only machine in the world capable of colliding beams of heavy ions. Since its first successful operation in the summer of 2000, RHIC has continued to operate every year to date.

RHIC was built at Brookhaven National Laboratory and is located on Long Island, New York. The machine is a 2.4 mile long loop with two rings of accelerating magnets inside that create two separate beams of heavy ions. The two separate beams travel around the loop in opposite

directions and are allowed to intersect at six points. The six intersection points of the two rings are where the beams of heavy ions can collide. When RHIC first began operation there were four separate experiments simultaneously collecting data from the heavy ion collisions. Each of the experiments was located at one of the six intersecton points. The abbreviated names of these original experiments are STAR, PHENIX, PHOBOS, and BRAHMS. STAR and PHENIX continue to collect data today, but PHOBOS and BRAHMS completed their collection of data in 2005 and 2006.

To date RHIC has created collisions from many different collision systems. The various collision systems are listed as follows: *p*+*p*, d+Au, Cu+Cu, Au+Au, Cu+Au, *p*+Al, U+U, and *p*+Au (*p*-proton, d-deuteron, Cu-copper nuclei, Au-gold nuclei, Al-aluminum nuclei, U-uranium nuclei). The heavy ion beams in RHIC can be accelerated to different speeds depending on the desired energy for the collisions. The highest center of mass energy for heavy ion collisions in RHIC for Cu+Cu, Au+Au, and d+Au has been 200 GeV per nucleon pair ($\sqrt{s_{NN}}$). For $p + p$ collisions RHIC has reached energies as high as $\sqrt{s_{NN}}$ = 510 GeV. RHIC collisions occur thousands of times per second allowing the experiments at RHIC to record millions or billions of collision events for each data set.

RHIC's heavy ion beams are created by a pre-injector system that consists of a source of nuclei and a series of smaller particle accelerators. RHIC and its pre-injector system are shown in Figure 4 [7]. The Electron Beam Ion Source (EBIS) supplies heavy ion beams and the Linear Accelerator (Linac) supplies protons [8]. EBIS can supply ion beams from almost any element. The atoms are initially ionized when they are shot through a foil that strips some of their electrons. The Booster Synchrotron is a circular accelerator that uses radio frequency electromagnetic waves to speed protons and ions up to about 37% the speed of light after receiving them from Linac or EBIS. More electrons are stripped when the ion beams leave the Booster Synchrotron and enter the Alternating Gradient Synchrotron (AGS). AGS then accelerates them in a similar way until they reach speeds of 99.7% the speed of light. The last of the electrons are stripped when the beam leaves AGS, leaving only the bare nuclei with large positive electric charges. The AGS-to-RHIC

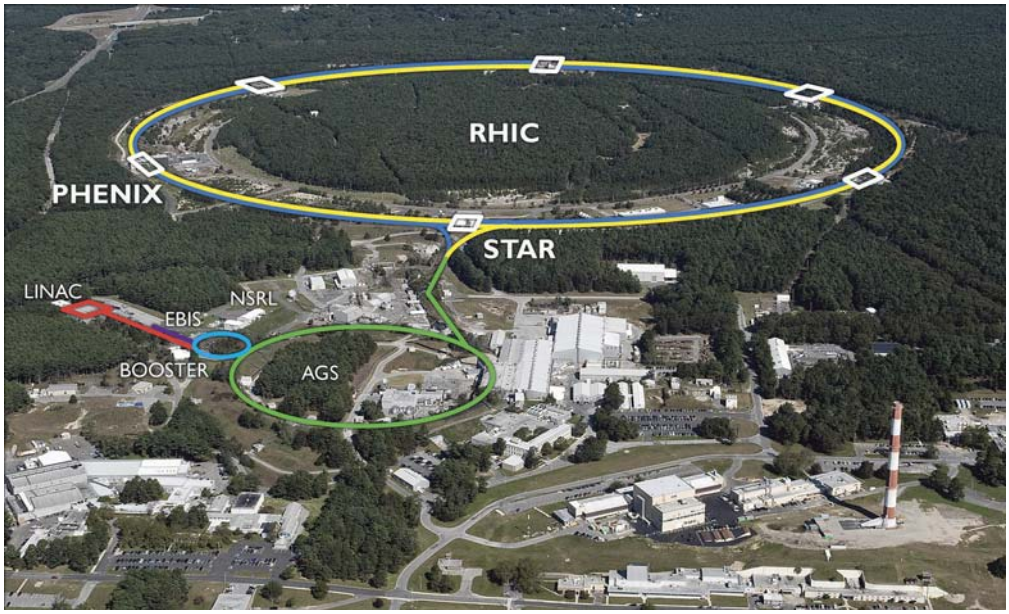

Figure 4: This is an aerial view of RHIC and its pre-injector system at Brookhaven National Laboratory. EBIS is the source of heavy ions and LINAC is the source of protons used in RHIC experiments. The Booster Synchrotron and AGS are two smaller particle accelerators that are used in series to speed up the heavy ions to 99.7% the speed of light before they are sent into RHIC. The yellow and blue circles outline RHIC's two separate beam lines. At six points along the circumference of RHIC the two beam lines intersect. These points are shown by the six white boxes drawn along the beam lines. PHENIX and STAR, the two remaining experiments at RHIC, are labeled and located at two of these points.

Line receives ions from AGS and uses a switching magnet to send ions down one of RHICs two beam lines. RHIC then accelerates the particles to about 99.995% the speed of light using its rings of superconducting magnets, increasing the kinetic energy of the beams by about eight times as much.

2.2 The Solenoidal Tracker at RHIC (STAR)

The medium produced by heavy ion collisions at RHIC is extremely short lived (approximately 10^{-23} seconds). Even for collisions with high enough temperature and baryon density for QGP formation, partons will only interact freely for a very short period of time before the medium cools and hadronization occurs. The only information about the parton interactions is carried away by the emitted hadrons. Therefore, to study those interactions we must gather as much information as possible about the emitted hadrons. The Solenoidal Tracker at RHIC (STAR) was built for this

purpose.

STAR is a giant solenoid magnet with a collection of detectors built inside. A solenoid magnet is a cylindrical coil of conducting material with an electric current running through it. The STAR solenoid magnet requires 4500 Amps in the main coil, and about 2000 Amps in the endcap coils. Solenoid magnets are useful because of the nearly constant magnetic field that they produce in the volume enclosed by their coils. The STAR solenoid magnet produces a 5000 Gauss magnetic field to within 50 Gauss in the radial direction and 3 Gauss in the azimuthal direction [9]. The entire STAR system weighs over 1,200 tons and is about three stories high. The main detector within STAR is the Time Projection Chamber (TPC). The TPC is a large cylinder that surrounds the beam line and measures 4.2 meters in length and 4 meters in diameter [10]. Several other detectors are built around the TPC to collect as much data from each collision as possible. We only use data collected by the TPC for this project, however other detector systems, such as the Time of Flight (TOF) detector, may be useful for future studies.

Figure 5 is a cutaway view of the STAR system [11, 12]. Beams of heavy ions will enter STAR from both sides and collide in the center. The Silicon Vertex Tracker is the closest detector to the beamline and is used for high precision hits. The Time Projection Chamber (TPC) is the large cylindrical chamber surrounding the beamline. The TPC is used to track particles produced by collisions. Outside of the TPC is the Time of Flight (TOF) detector, used to record the velocity of particles. Outside of the TOF is the Electromagnetic Calorimeter, used to record information about high energy electrons, muons, and photons. The coils of the solenoid magnet are at the outside of the entire system. To the left and right of STAR are electronics platforms which help to show the size of the machine.

2.2.1 The Time Projection Chamber (TPC)

The purpose of the TPC is to track particles, measure their momenta, and record their ionization energy loss, a useful value for identifying particles. The TPC is filled with P10 gas (10% methane, 90% argon), slightly above atmospheric pressure. When charged particles travel through the TPC

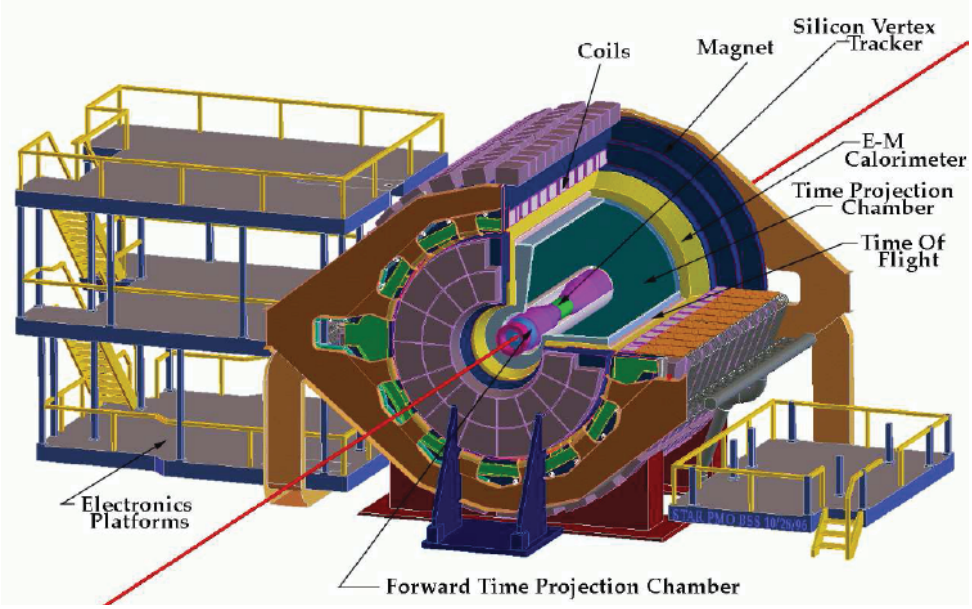

Figure 5: Shown is a cutaway view of the STAR detector. The beamline is shown in red going through the center of the detector.

they ionize nearby gas molecules leaving behind a trail of free electrons. The electrons on each half of the TPC are forced to drift to the end caps due to an external electric field created by the TPC's 20 kV cathode [13]. The end caps of the TPC consist of anode wires and detector pads that record the drifting electrons. When an electron nears an anode wire it experiences a large force and ionizes many of the gas molecules around it creating a cluster of charge. An image charge is created on the detector pad and is recorded as a "hit." All the hits for a particle are added together to create a "track" for that particle. This allows us to use the TPC to recreate the trajectories of particles. We can more accurately recreate the trajectories of particles with many hits, as opposed to those with few hits. Figure 6 is of the reconstructed paths of particles from a single Au+Au collision detected by the TPC [12].

Charged particles traveling through the TPC travel in helical trajectories due to the magnetic field produced by STAR's solenoid magnet. Using the radii of the helical trajectories allows the us to determine the momenta of those particles. Charged particles with opposite charges will curve in opposite directions when traveling through the magnetic field. The direction of curvature for each particle allows us to determine whether the particle is positively or negatively charged. Neutral

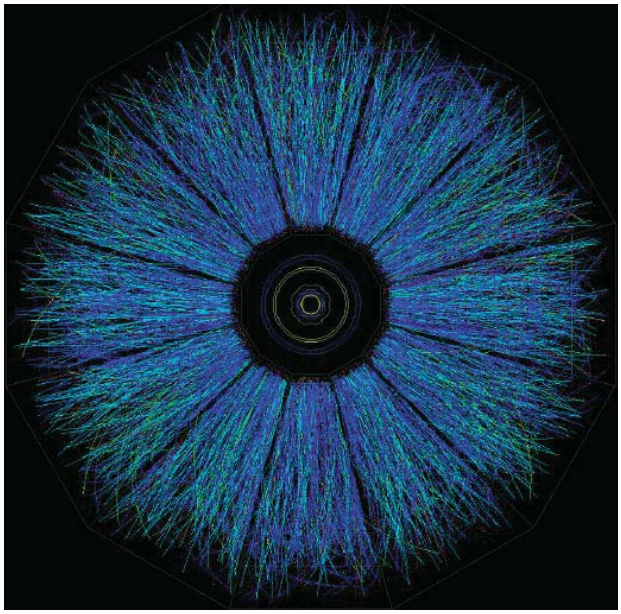

Figure 6: Shown are approximately 5,000 reconstructed tracks of particles detected by the TPC from a single Au+Au collision. The tracks are shown from a beams eye view with each line representing a tracked particle. High momentum tracks are represented by red lines and curve less than the low momentum tracks represented by blue lines. There are many more low momentum tracks than high momentum tracks.

particles are not detected directly by the TPC, but may decay into charged particles that are. Those charged particles can then be used to reconstruct the neutral particle from which they came.

As seen in Figure 6, thousands of particles can be produced from a central heavy ion collision. The TPC records information about each particle which we use to determine information about the collision event as a whole. We determine a value related to the number of particles produced by the collision known as the "reference multiplicity." Reference multiplicity is correlated to the centrality of the collsion. The most central collisions will have the highest reference multiplicities and collisions of heavier nuclei, such as Au+Au, will usually have higher reference multiplicities than collisions of smaller nuclei, such as Cu+Cu. We also determine an approximate point where the collision occurred. This point is known as the "primary vertex" and is the point to which all the particles tracked within the TPC trace back. The primary vertex is usually near the center of the TPC, but can be off center along the beam line towards either end of the TPC by as much as half a meter.

Many hadrons will decay within the TPC. The hadrons that are emitted by a heavy ion collision should trace back to within 3 cm of the primary vertex. These tracks are known as "primaries" and have the primary vertex added as another hit for the determination of their momenta. A particle that is produced by a decay of a heavier particle is known as a "daughter." The particle that produced a daughter is known as the "parent." As primaries decay, their daughters may not trace back to within 3 cm of the primary vertex depending how far their parent had travelled. These tracks are known as "secondary tracks." It may be difficult for us to distinguish between primary and secondary tracks. For this reason we maintain a double list of tracks for each event. The first list of tracks, known as "globals," include every track. Globals do not include the primary vertex as a hit. The second list of tracks are those that meet the criteria to be classified as a primary. Primaries include the primary vertex as a hit.

2.2.2 Particle Identification

As discussed above, the TPC can record data that we can use to determine the charge, momentum, and specific ionization energy loss of each charged particle traveling through the chamber. All charged particles leave behind a trail of ionized gas and free electrons which are recorded as hits by the detector pads at either end of the TPC. Ionization energy loss is directly measured for each particle in this process so that it can be used for particle identification. Particles are able to be identified statistically due to a correlation between their ionization energy loss and momentum. This method of particle identification is known as the Bethe-Bloch method [14].

For the Bethe-Bloch method it is important to note that particles cannot be identified with perfect accuracy. When their ionization energy losses are plotted against their momenta, the particles tend to fall along different bands according to their identity as shown in Figure 7 [15]. The cross-section of each band is approximately a Gaussian distribution that falls off towards the outer edges of the band. This means that statistically particles are most likely to be at the center of their band but many will be slightly off to either side. This gives each band a width. A few outlier particles may be completely off from their bands. At certain ranges of momentum, some bands approach

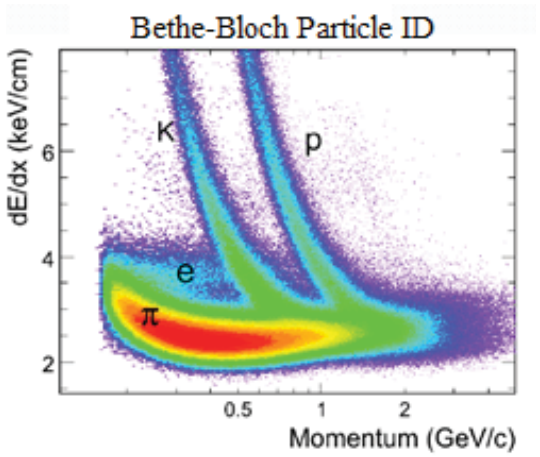

Figure 7: The Bethe-Bloch Method uses correlations between ionization energy loss (dE/dx) and momentum to identify particles. Protons (p), kaons (K), electrons (e), and pions (π) are represented in the plot. Color represents the amount of particles that are along each line. Red being the most and violet being the least.

each other and may cross. In these ranges it is not possible to clearly identify which band a particle belongs to. At higher momenta, the Bethe-Bloch bands merge together and clear particle identification is no longer possible.

3 Delta Baryons and Statistical Analysis Methods

In order to contribute to the study of heavy ion collisions and parton interactions, we have chosen to focus on a specific type of hadron emitted by the collisions. These hadrons are known as "delta baryons." There are many different delta baryons distinguished by their different masses and charges. The delta baryons that we are studying have an accepted mean mass of 1232 MeV/c^2. The four charge states of delta baryons are minus one, zero, plus one, and plus two. For this project, we are studying the plus two charge state, commonly referred to as the "doubly-charged" delta baryon. We are also studying the anti-particle of the doubly-charged delta baryon. The anti-particle has a minus two charge. For simplicity in this paper, when referring to doubly-charged delta baryons with an accepted mass of 1232 MeV/c^2 we use the greek uppercase letter "Δ" (pronounced delta). When referring to the anti-particle of the Δ, we use "$\overline{\Delta}$" (pronounced delta-bar). Placing a bar over a particle's symbol is the standard notation used to denote its anti-particle.

3.1 Interest in the Delta Baryon (Δ)

Δ's are commonly produced in heavy ion collisions because of their quark content. The quark content of the Δ is three up quarks, the lightest of the six flavors of quarks. With each up quark having a positive charge of two-thirds the charge of an electron, the Δ has an overall positive charge of twice the charge of an electron. The $\overline{\Delta}$ is therefore composed of three up antiquarks, and has an overall negative charge of twice the charge of an electron. Δ's may be produced by the up quarks already present in the nuclei before the collision. However, $\overline{\Delta}$'s may only be produced by up antiquarks that are created during the collision. For this reason, $\overline{\Delta}$'s are expected to be less common than Δ's.

Due to their charge and their mass, Δ's are only able to decay through a single decay channel. When a Δ decays the daughters it produces are a proton and a pion. Both Δ's and protons are baryons, while pions are mesons. With one baryon before and after a Δ decay, baryon number is conserved as it must be. The proton and pion both carry away equivalent positive charge, accounting for the double charge of the Δ. Protons have a mass of about 938 MeV/c^2 and pions have a mass of about 140 MeV/c^2, with a combined mass of about 1078 MeV/c^2. Any of the Δ's mass that is not invested into the masses of the proton and pion is invested into their kinetic energy. A diagram of a Δ decay is shown in Figure 8.

3.1.1 Δ Yield Modifications

Δ's belong to a group of hadrons known as "resonances," and are often referred to as "delta resonances." Resonances are a specific subcategory of hadrons that have extremely short mean lifetimes. Δ's have such short mean lifetimes (approximately 10^{-23} seconds) because they decay via the strong nuclear force, the strongest of the fundamental forces. The short mean lifetime of resonances makes them useful for studying effects within the collision medium which is short lived as well [16]. The Δ is of particular interest for studying the intensity of the interactions within the collision medium because of how close its mean lifetime is to the predicted time for QGP formation.

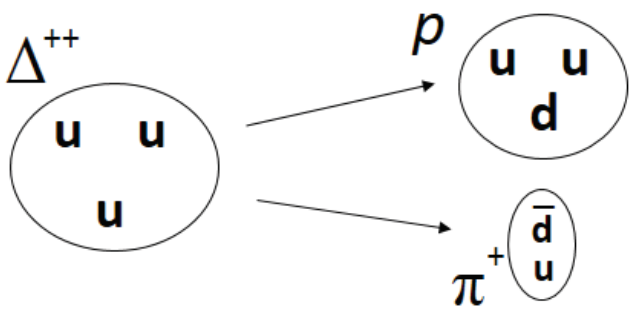

Figure 8: Shown is a diagram of a Δ decay. Each Δ will decay, via the strong nuclear force, into a proton (p) and a positively charged pion (π^+). This is the only decay channel of the Δ. Protons are baryons and pions are mesons so baryon number is conserved. The proton and pion each have half the charge of the Δ so electric charge is also conserved. Up quarks are represented by "u," down quarks are represented by "d." and down antiquarks are represented by "$\overline{d}$." Quark content is conserved because the down quark in the proton is produced as a partner with the down antiquark in the pion. Quarks content is always conserved for decays via the strong nuclear force.

The ratios of the particles produced by a heavy ion collision are set once the system reaches chemical freeze-out. This means that on average the numbers of each type of partcle will not change. Particles in the medium continue to interact inelastically until the system reaches kinetic freeze-out. When a particle decays, its daughters are initially correlated to each other. However, if the daughters interact inelastically within the medium, the correlation to each other will be lost. Resonances with mean lifetimes short enough can decay inside the medium before it reaches kinetic freeze-out. For these resonances, the correlation between their daughters may be lost and we will be unable to reconstruct their decay.

Depending on when the collision medium reaches kinetic freeze-out, the measured yield of Δ's may be reduced from the expected yield at chemical freeze-out. This is determined by the time interval between chemical and kinetic freeze-out of the collision medium. If this time interval is longer than the mean lifetime of Δ's, a reduction of measured Δ yield is expected. Because stable particles do not decay, their measured yield should be consistant with their yield at chemical freeze-out regardless of when kinetic freeze-out occurs. By comparing the yield of Δ's to stable particles, such as protons, it is possible to gain information about the time interval between chemical and kinetic freeze-out. If the ratio of Δ's to protons is reduced from what is predicted, the time interval must be longer than or near to the mean lifetime of the Δ. If the ratio of Δ's to protons is unaffected,

the time interval must be shorter than the mean lifetime of the Δ. This comparison can be done for Δ's in different centrality collisions to study the dependence of the lifetime of the collision medium on collision size.

3.1.2 Δ Mass and Width Modifications

Due to the short mean lifetime of the Δ and Heisenberg's uncertainty principle, there is a large variation in the mass of each Δ. Heisenberg's uncertainty principle describes an inverse correlation between uncertainty in time and uncertainty in energy. If the uncertainty in time is small, then the uncertainty in energy, or mass, must be large. The uncertainty of the Δ's mean lifetime is small, so therefore there must be a large uncertainty in the Δ's energy, which is reflected in its mass. Proton's are stable particles so their mean lifetime is infinite, therefore the uncertainty in the mass of a proton is zero. The Δ mass of 1232 MeV/c^2 is the accepted mean mass of the distribution of Δ's [17]. The full width of the mass distribution is simply referred to as "width." The width of the Δ is accepted to be 117 MeV/c^2 [17].

In 2008, STAR published a shift in the mean mass of the Δ for *p*+*p* and *d*+Au collisions [18]. A possible explanation given for the mean mass shift was that the Δ decay daughters may be rescattering with other particles causing a phase space distortion. The width of the Δ mass distribution did not show any distortion. By studying Δ's in Cu+Cu collisions we are able to study how modifications of the mean mass may be related to the centrality of heavy ion collisions. We are also able to study the mass shifts at higher momenta. This is due to higher statistics and the larger yield of Δ's produced in the Cu+Cu system than what was available in the *p*+*p* and *d*+Au systems.

3.2 Reconstruction and Combinatoric Background Subtraction

To study Δ's in Cu+Cu collisions, we first completed a statistical analysis of the STAR data. This analysis required me to write 12 macros containing approximately 5600 lines of C++ code. These macros were used to perform data reduction, Δ decay reconstruction, mass peak and spectral fitting, determination and application of efficiency and acceptance corrections, and determination

of systematic errors.

Because Δ's are so short lived they never travel far enough to make it into the TPC where they can be detected directly. Particles must travel about 50 cm from the primary vertex to be detected by the TPC, Δ's may only travel a few femtometers before decaying. As discussed above, the information about each Δ decay is carried away by its proton and pion daughters. Protons and pions do travel far enough and are detected by the TPC. To study Δ's, we extract their information from the properties of their proton and pion daughters.

Due to the physical laws of conservation of energy and conservation of momentum, the combined energy and momentum of the daughters of a Δ decay must equal the original energy and momentum of the Δ. Therefore, we use the measured energy and momenta of proton and pion daughters to determine the energy and momentum of their Δ parent. This is known as "reconstruction" and allows us to recreate Δ's from their daughters. Knowing the energy and momentum of a Δ means that we also know the Δ's "invariant mass." Invariant mass is the mass of a particle in its rest frame. Due to special relativity and the high velocity of particles created in heavy ion collisions, the mass of particles will not be the same in different reference frames. Using invariant mass avoids this confusion.

Every proton and pion that is classified as a primary track has a chance of being the decay daughter of a Δ. For each collision, we take all primary protons and primary pions and match them into all possible combinations. We refer to these proton-pion pairs as "Δ candidates." We then determine the invariant mass of each Δ candidate and fill it into a histogram to create a mass distribution. Clearly not all Δ candidates within the mass distribution are actual Δ's. Most of the Δ candidates are created from protons and pions that did not come from the same Δ or came from a different source within the collision. These pairs are known as "combinatoric background." We refer to the difference between the combinatoric background and the original Δ candidate mass distribution as the "signal."

Our objective is to isolate the Δ signal so that we can measure the properties of Δ's, such as their mean mass, width, and yield. To meet our objective we must be able to subtract the

combinatoric background from the Δ candidate mass distribution so that we our only left with the Δ signal. This is possible due to the high statistics available in the STAR data sets. We use over 24 million collisions for our analysis of the Cu+Cu system. The combinatoric background is created from uncorrelated pairs of protons and pions emitted by heavy ion collisions. With a large enough sample of any uncorrelated pairs of protons and pions produced by the same collisions, we can recreate the combinatoric background mass distribution. Then we can subtract it from the Δ candidate mass distribution and isolate the Δ signal. We have two methods to recreate the combinatoric background.

The first of these methods is the "rotation method," developed by Dr. Witt. This method recreates the combinatoric background by first breaking the correlation of any Δ decay daughters within a collision. These now uncorrelated proton-pion pairs are then combined, along with other uncorrelated pairs, to recreate the combinatoric background. To break any correlations, we rotate the transverse momentum (p_T) vectors of all the protons about the beam line. p_T is the component of momentum that is perpendicular to the beam line. The p_T vector of each proton is randomly placed within a narrow 10 degree window that is 180 degrees from its original direction. This preserves the symmetry of the collision, but changes the orientation of protons to pions. The correlations between the protons and pions are broken, and the pairs are combined to recreate the combinatoric background. The combinatoric background is then subtracted from our Δ candidate mass distribution to isolate the Δ signal.

The second of these methods is the "mixed event method." This method takes protons from one collision and matches them with pions from a different collision. Because the protons and pions come from different collisions it is guaranteed that they are not correlated from a Δ decay. We must carefully match collision events to ensure that proton-pion pairs from mixed events are the same as pairs from within single events. To do this, we only mix events that are nearly the same. The events are required to have similar primary vertices along the beam line and similar centralities. The primary vertices must not be separated by more than 2 cm along the direction of the beam line and the reference multiplicities must be within about 5% of each other. Reference multiplicity is taken

to be proportional to the centrality of collisions, so collisions with similar reference multiplicities will have similar centrality. The proton-pion pairs from matching events are combined to recreate the combinatoric background, which is then subtracted from the Δ candidate mass distibution to isolate the Δ signal.

3.3 Cuts

Making "cuts" means that we remove data from our analysis that is likely to add "noise" to the desired signal. Noise is any residual background that is not subtracted with the combinatoric background. Noise may be caused by many different sources. We begin by making cuts on events, then on particle tracks, and finally on Δ candidates.

The primary vertex point is referenced to a set of axes within STAR such that the beam line represents the z-axis, the y-azix is up, and the x-axis points towards the center of the RHIC loop. The TPC acceptence varies depending where along the z-axis the primary vertix is. Events that are too far from the center of the TPC have poor acceptance on one half of the chamber. For this reason, we cut events with a primary vertex that is further than 50 cm from the center of the TPC along the z-axis. We also cut events with a reference multiplicity less than 19 because these events do not create enough particle tracks to be useful for our analysis. The events with a reference multiplicity of 19 or greater are divided into six centrality bins, each with the same number of events. Event selection plots are shown in Figure 9.

For track selection we made cuts for track quality and particle identification. To ensure track quality we only used tracks with a ratio greater than 0.52 for recorded TPC hits over possible TPC hits. This cut eliminates split tracks which occur when the tracking software creates two separate tracks out of a single track. We also cut tracks with a rapidity greater than 0.5 or less than -0.5. Rapidity is dependent on momentum parallel to the beam line. Particles with a high absolute value of rapidity will be more parallel to the beam line, while particles with a low absolute value of rapidity will be nearly perpendicular to the beam line. This rapidity cut requires tracks to be more perpendicular to the beam line and closer to the center of the TPC.

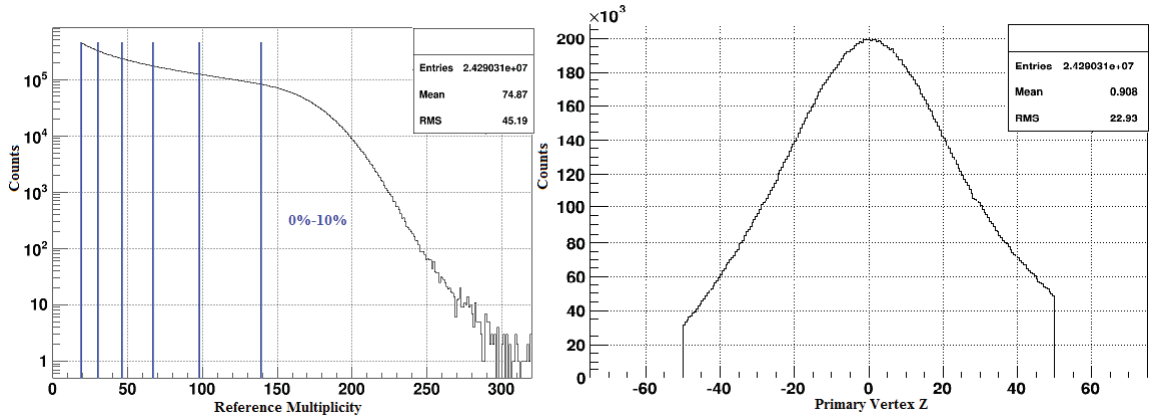

Figure 9: The histogram on the left shows the reference multiplicity of the events used for our analysis. Events with a reference multiplicity less than 19 were cut. The blue lines separte the six different centrality bins. The most central bin represents 0%-10% centrality. Events in this bin are the top 10% most central events. The next five bins each represent the next 10% of events all the way out to 60% centrality. The histogram on the right shows the primary vertex along the z-axis of events used in our analysis. The z-axis in the TPC runs parallel to the beam line. Events with a primary vertex z greater than 50 cm or less than -50 cm were cut.

The most important track cuts were made to solve issues with particle identification. When using the Bethe-Bloch method, we initially treated all tracks within two standard deviations of the proton band as protons and all tracks within two standard deviations of the pion bind as pions. For a Gaussian distribution, two standard deviations includes about 95%. With only these track cuts there was a significant amount of residual background within the Δ signal for higher momentum bins. However, the Δ signal in lower momentum bins was very clean and did not have issues with noise. For this reason, we tightened the particle identification cuts. Tracks within two standard deviations of the proton band are treated as protons unless they are within one standard deviation of the pion band. Tracks within two standard deviations of the pion band are treated as pions unless they are within one standard deviation of the kaon band. These cuts reduced the amount of pions being misidentified as protons and kaons being misidentified as pions. The significant noise in the higher momentum bins of the Δ signal went away. This led us to conclude that the noise was caused by misidentified particles.

We made three cuts on Δ candidates. The first of these cuts was to ensure that the momentum of the proton was greater than the momentum of the pion. Protons are much heavier than pions and

will have a greater momentum than the pion when produced in a Δ decay. Therefore, any proton-pion pairs considered in our analysis must have the proton with greater momentum than the pion. The second cut is on the opening angle of proton-pion pairs. This cut removes Δ candidates with an opening angle between them less than 0.2 radians or an opening angle greater than 1.8 radians. Δ candidates with an opening angle greater than 1.8 radians are cut because real Δ's will usually have a smaller opening angle due to their high velocities in the expanding collision medium. Δ candidates with an opening angle less than 0.2 radians are cut to avoid an over subtraction from the rotation method. Tracks may be rotated over the top of each other creating orientations that do not occur in heavy ion collisions as frequently.

The third cut is referred to as the dip angle cut and removes proton-pion pairs with very similar momenta[19]. The equation used for the dip angle is given as

$$\cos(dipAngle) = \frac{p_{T\pi}p_{Tp} + p_{z\pi}p_{zp}}{p_\pi p_p}, \tag{1}$$

where p_T is transverse momentum, p_z is momentum along the z-azis, and p is total momentum. The p and π subscripts on these terms indicate that they are either proton or pion properties. Proton-pion pairs with a dip angle less than 0.04 radians are cut using Equation 1. Similar to the narrow opening angle cut, the dip angle cut reduces over subtraction caused by the rotation method by rotating tracks over the top of each other. All cuts are summarized in Table 1.

Cut Description	**Accepted Values**
Primary Vertex Z (PVZ)	$\lvert$PVZ$\rvert < 50$ cm
Reference Multiplicity	> 19
N_{Hits} / $N_{HitsPossible}$	> 0.52
Track Rapidity	$\lvert$Rapidity$\rvert < 0.5$
Protons $\lvert N_{\sigma p}\rvert$	< 2.0
Protons $\lvert N_{\sigma \pi}\rvert$	> 1.0
Pions $\lvert N_{\sigma \pi}\rvert$	< 2.0
Pions $\lvert N_{\sigma K}\rvert$	> 1.0
Δ Decay Opening Angle	> 0.2 rad and < 1.8 rad
Δ Dip Angle	> 0.04 rad
Δ Daughter Momenta	$p_p > p_\pi$

Table 1: Events, Tracks, and Δ Candidates are required to pass these cuts in our analysis.

4 Yield, Mass, and Width Determination for Delta Baryons

4.1 Relativistic Breit-Wigner Fits

To study the physics involved in Δ production within Cu+Cu collsions we fit the Δ mass peaks with a relativistic Breit-Wigner function times a phase space function. The fit function we use is from previous resonance studies done by the STAR collaboration [3, 18].

The relativistic Breit-Wigner function (BW) is a probability distribution function that describes the production of short lived resonances. The form of BW is given as

$$BW = \frac{Y M_{p\pi} M_0 \Gamma(M_{p\pi})}{(M_0^2 - M_{p\pi}^2)^2 + M_0^2[\Gamma(M_{p\pi})]^2}, \tag{2}$$

where $M_{p\pi}$ represents the invariant mass along the horizontal axis of the Δ mass peak. M_0 represents the mean invariant mass of the peak and *Y* is a constant proportional to the yeild of Δ's. $\Gamma(M_{p\pi})$ is a function that represents mass dependent width and is given as

$$\Gamma(M_{p\pi}) = \frac{\Gamma_0 M_0}{M_{p\pi}} \times \frac{k(M_{p\pi})^3 F(\Lambda_\pi, k(M_{p\pi}))^2}{k(M_0)^3 F(\Lambda_\pi, k(M_0))^2}. \tag{3}$$

In this function Γ_0 is the width of the Δ peak and Λ_π=R^{-1}, where R is the range of the strong interaction. In this case Λ_π is a constant given to be 290 MeV/c^2, which corresponds to an interaction range of R = 0.68 fm. $k(M_{p\pi})$ is the center of mass momentum of the pion-nucleon system [20]. Note that

$$M_{p\pi} = \sqrt{m_p^2 + k^2} + \sqrt{m_\pi^2 + k^2}, \tag{4}$$

where m_p and m_π are the proton and pion masses. Solving for k in terms of $M_{p\pi}$ yields

$$k(M_{p\pi})^2 = \frac{(M_{p\pi}^2 - m_p^2 - m_\pi^2)^2 - 4m_p^2 m_\pi^2}{4M_{p\pi}^2}. \tag{5}$$

$F(\Lambda_\pi, k(M_{p\pi}))$ is the form factor used to fit the nucleon-pion scattering phase shift

$$F(\Lambda_\pi, k(M_{p\pi})) = \frac{\Lambda_\pi^2}{\Lambda_\pi^2 + k(M_{p\pi})^2}. \tag{6}$$

The phase space function (PS) comes from a Boltzmann distribution for emitted protons and pions and is given as

$$PS = \frac{M_{p\pi}}{\sqrt{M_{p\pi}^2 + p_T^2}} \times \exp\left(-\frac{\sqrt{M_{p\pi}^2 + p_T^2}}{T}\right). \tag{7}$$

In this function p_T is the average transverse momentum of the bin, and T is a constant that is historically related to the kinetic freeze-out temperature for the medium. For Au+Au and *p*+*p* collisions T is taken to be about 120 and 160 MeV [3]. For Cu+Cu collisions we take T to be 140 MeV.

With $BW \times PS$ we have three fit parameters. These parameters are *Y*, Γ_0, and M_0. We also add a gaussian (RBG) to our fit function to describe any residual background that may be present. The form of RBG is

$$RBG(M_{p\pi}) = A \times \exp\left(-\frac{(M_{p\pi} - B)^2}{2C^2}\right), \tag{8}$$

where A is the gaussian amplitude, B is the gaussian mean, and C is the gaussian width. A, B, and C, are three more fit parameters that are included in our final fit function,

$$BW \times PS + RBG. \tag{9}$$

The Δ signal and $\overline{\Delta}$ signal extracted using the rotation method are each divided into six centrality bins and each centrality bin is divided into nine p_T bins. The fit results for the Δ signal are shown in Figures 10-15. The fit results for the $\overline{\Delta}$ signal are shown in Figures 16-21.

4.2 Relativistic Breit-Wigner Mass and Width

The relativistic Breit-Wigner mass and width values are taken directly from the fits shown in Figures 10-21. The rotation method used to subtract the combinatoric background does an excellent job of eliminating residual background. To get an estimate for the systematic error within our analysis, we also extracted Breit-Wigner mass and width values using the mixed event method. Within each p_T bin, we averaged the percent difference between mass and width values obtained using the rotation method and those obtained using the mixed event method. The averaged percent difference within a centrality bin was then applied as the systematic error for the data points within that bin.

The Δ and $\overline{\Delta}$ Breit-Wigner masses determined in our analysis of 200 GeV Cu+Cu collisions are shown in Figure 22. For all six centrality bins, and for both Δ's and $\overline{\Delta}$'s, there is an average

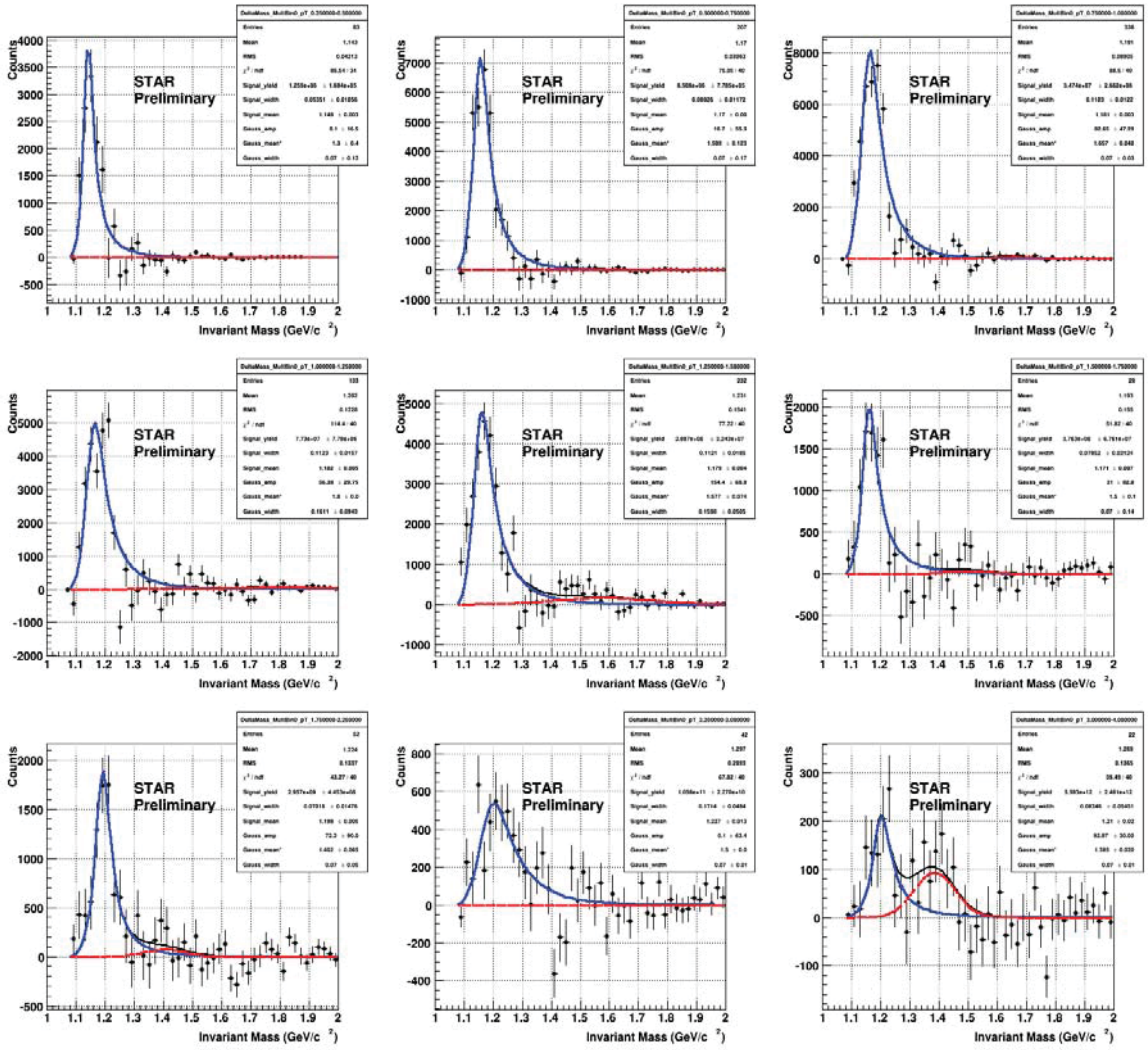

Figure 10: Shown are the relativistic Breit-Wigner fits of the Δ invariant mass distribution for 50%-60% centrality. The Δ signal was obtained using the rotation method. The centrality bin is divided into 9 p_T bins. Lowest to highest p_T appear left to right then top to bottom. The solid blue line fits the signal, while the red line is the Gaussian function that is used to account for any residual background.

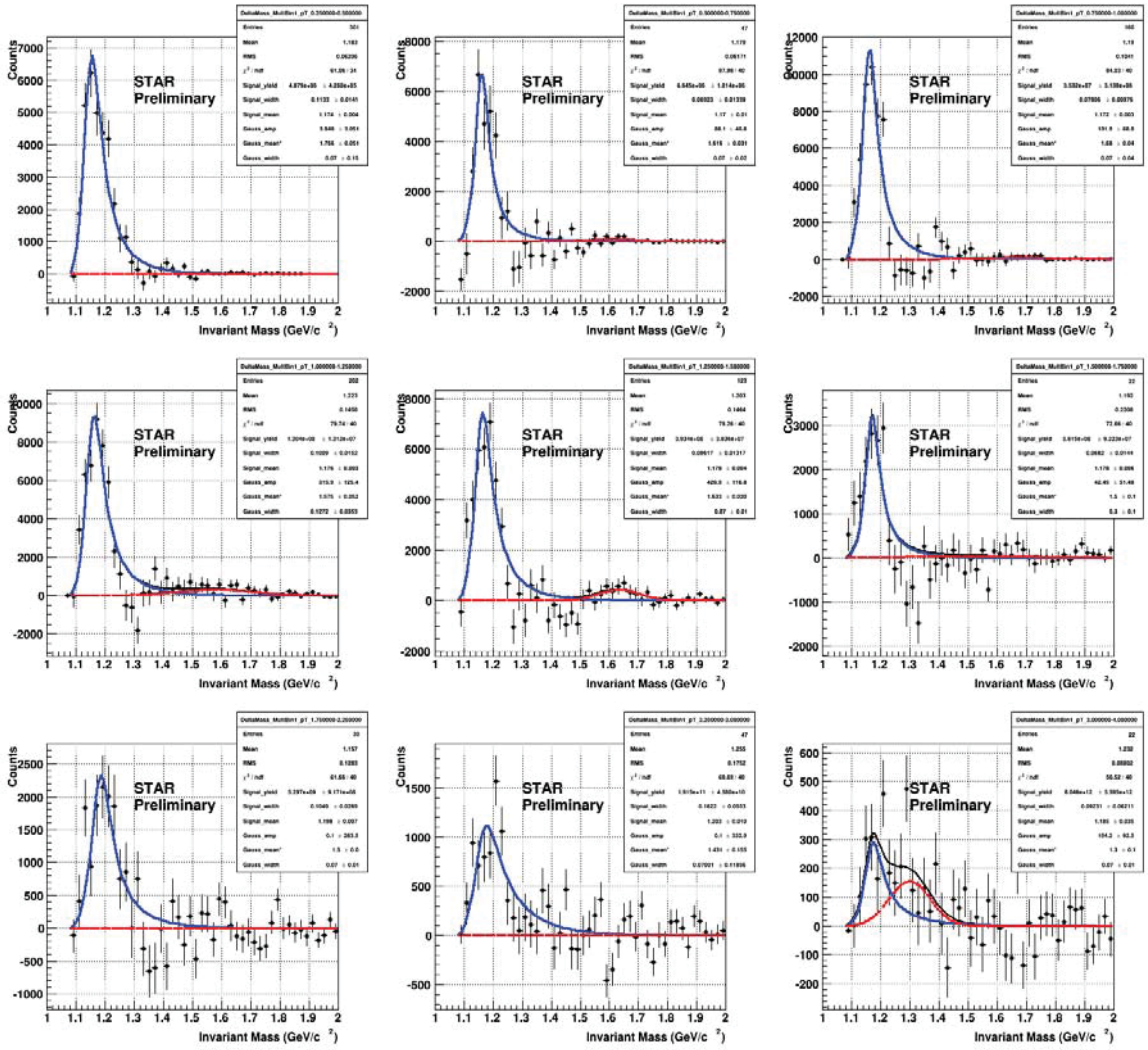

Figure 11: Shown are the relativistic Breit-Wigner fits of the Δ invariant mass distribution for 40%-50% centrality. The Δ signal was obtained using the rotation method. The centrality bin is divided into 9 p_T bins. Lowest to highest p_T appear left to right then top to bottom. The solid blue line fits the signal, while the red line is the Gaussian function that is used to account for any residual background.

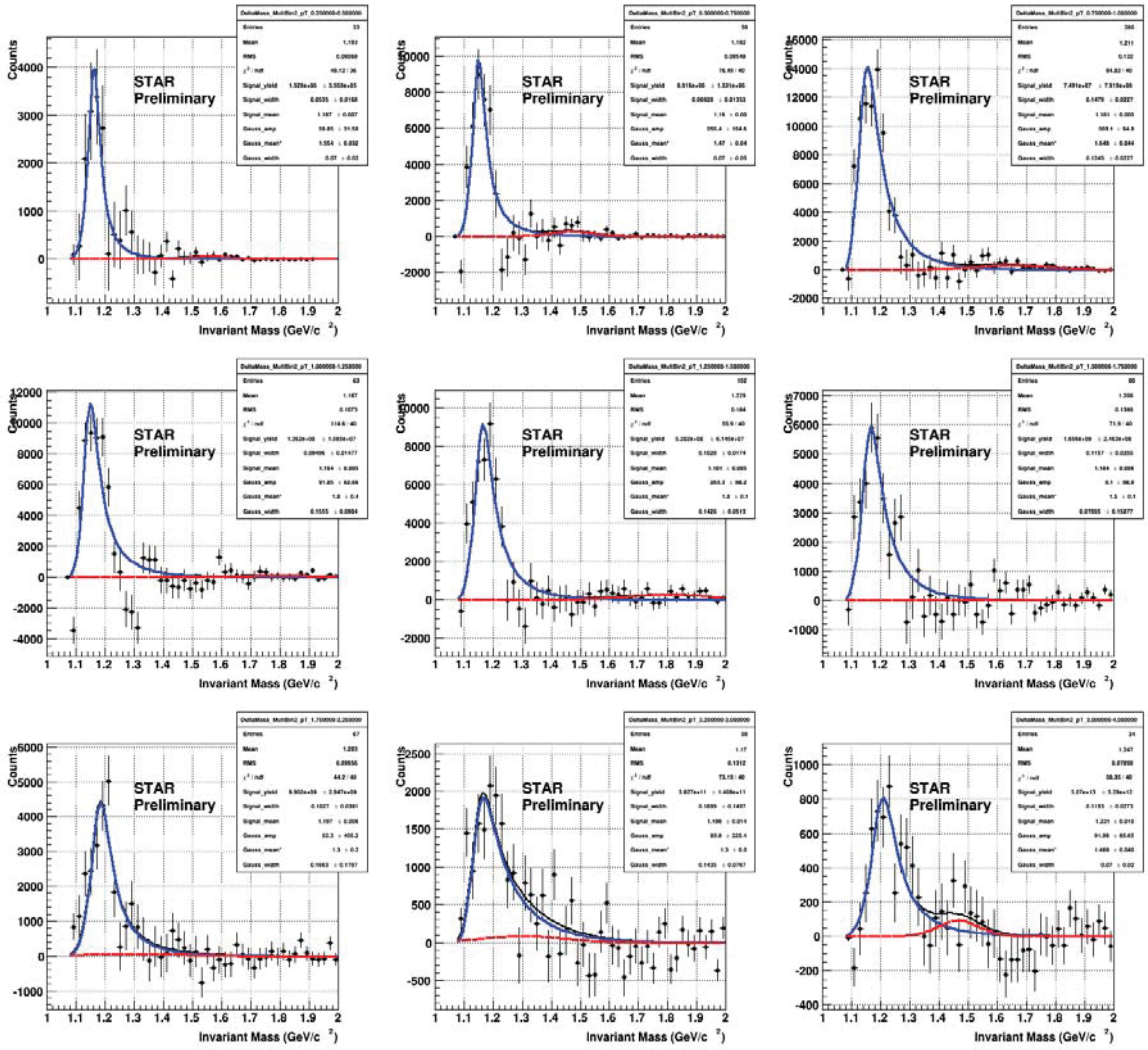

Figure 12: Shown are the relativistic Breit-Wigner fits of the Δ invariant mass distribution for 30%-40% centrality. The Δ signal was obtained using the rotation method. The centrality bin is divided into 9 p_T bins. Lowest to highest p_T appear left to right then top to bottom. The solid blue line fits the signal, while the red line is the Gaussian function that is used to account for any residual background.

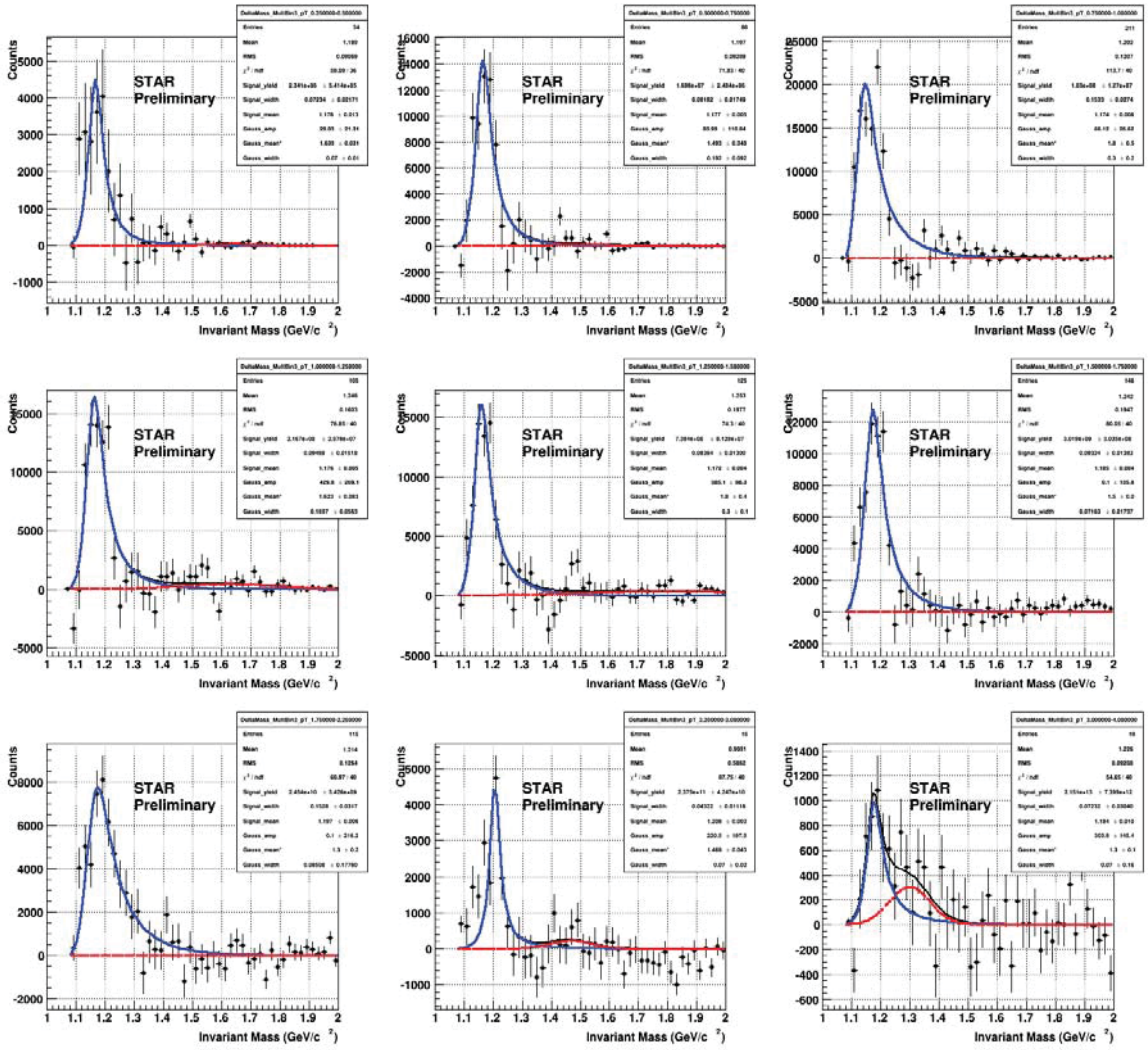

Figure 13: Shown are the relativistic Breit-Wigner fits of the Δ invariant mass distribution for 20%-30% centrality. The Δ signal was obtained using the rotation method. The centrality bin is divided into 9 p_T bins. Lowest to highest p_T appear left to right then top to bottom. The solid blue line fits the signal, while the red line is the Gaussian function that is used to account for any residual background.

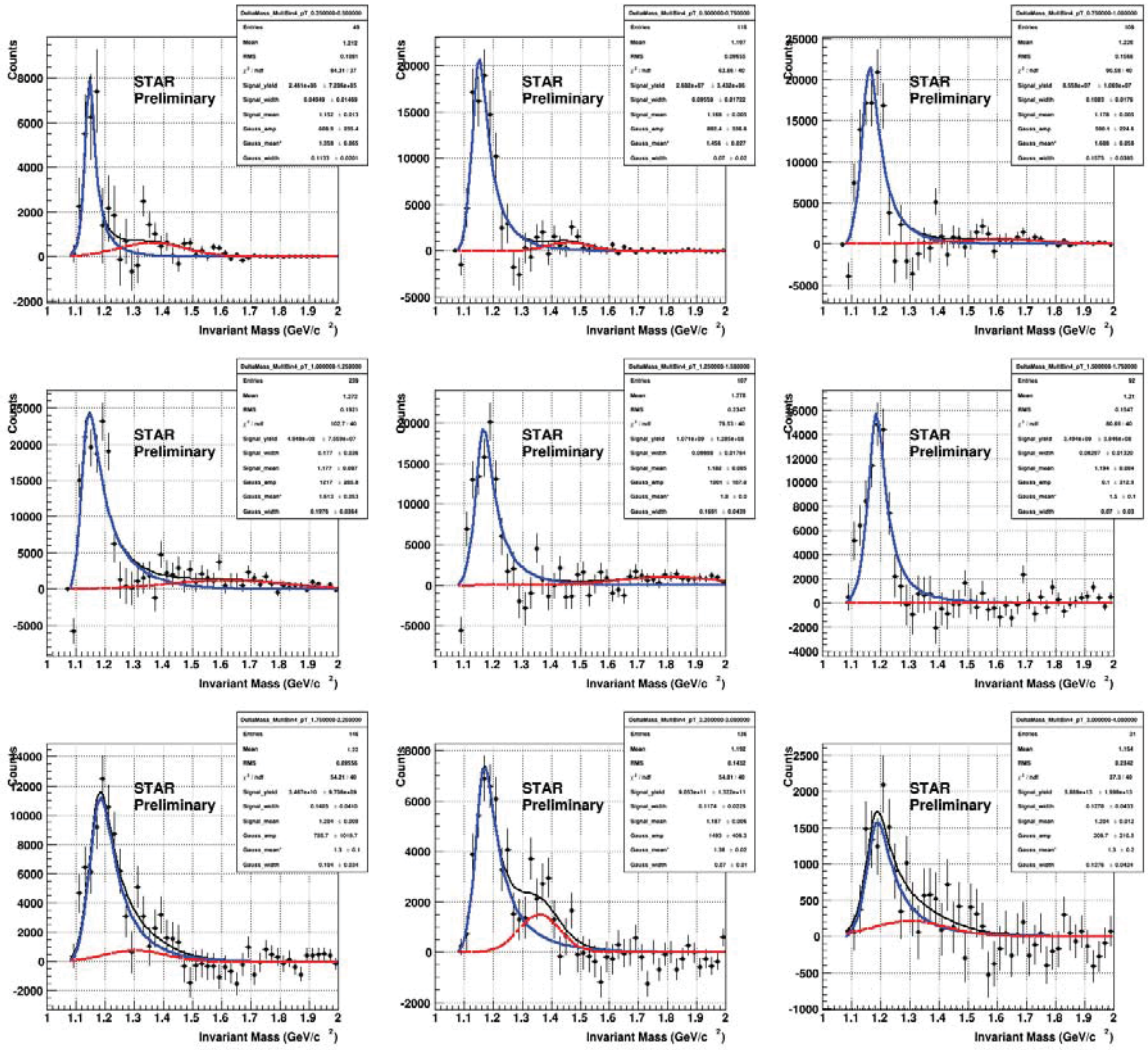

Figure 14: Shown are the relativistic Breit-Wigner fits of the Δ invariant mass distribution for 10%-20% centrality. The Δ signal was obtained using the rotation method. The centrality bin is divided into 9 p_T bins. Lowest to highest p_T appear left to right then top to bottom. The solid blue line fits the signal, while the red line is the Gaussian function that is used to account for any residual background.

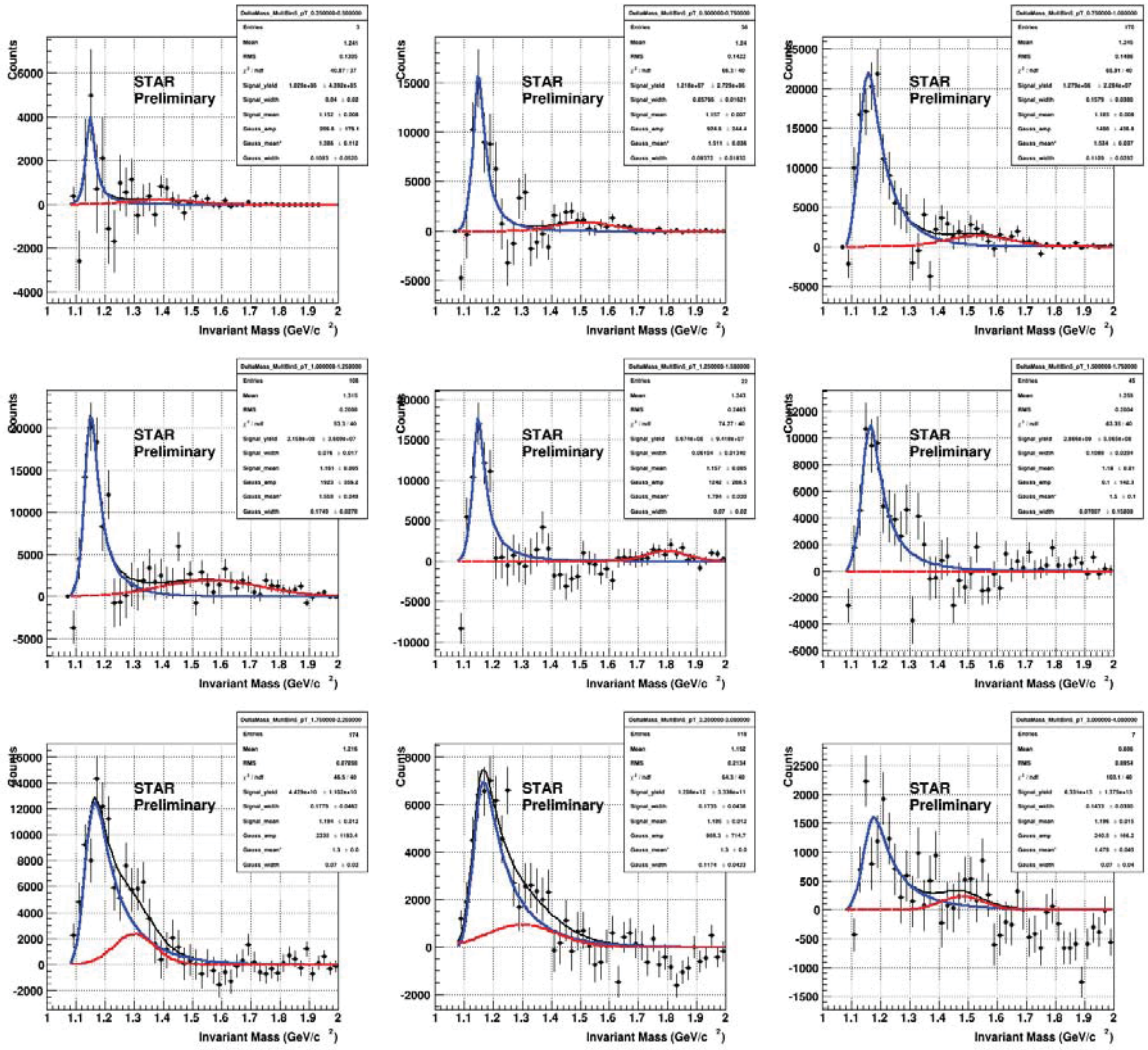

Figure 15: Shown are the relativistic Breit-Wigner fits of the Δ invariant mass distribution for 0%-10% centrality. The Δ signal was obtained using the rotation method. The centrality bin is divided into 9 p_T bins. Lowest to highest p_T appear left to right then top to bottom. The solid blue line fits the signal, while the red line is the Gaussian function that is used to account for any residual background.

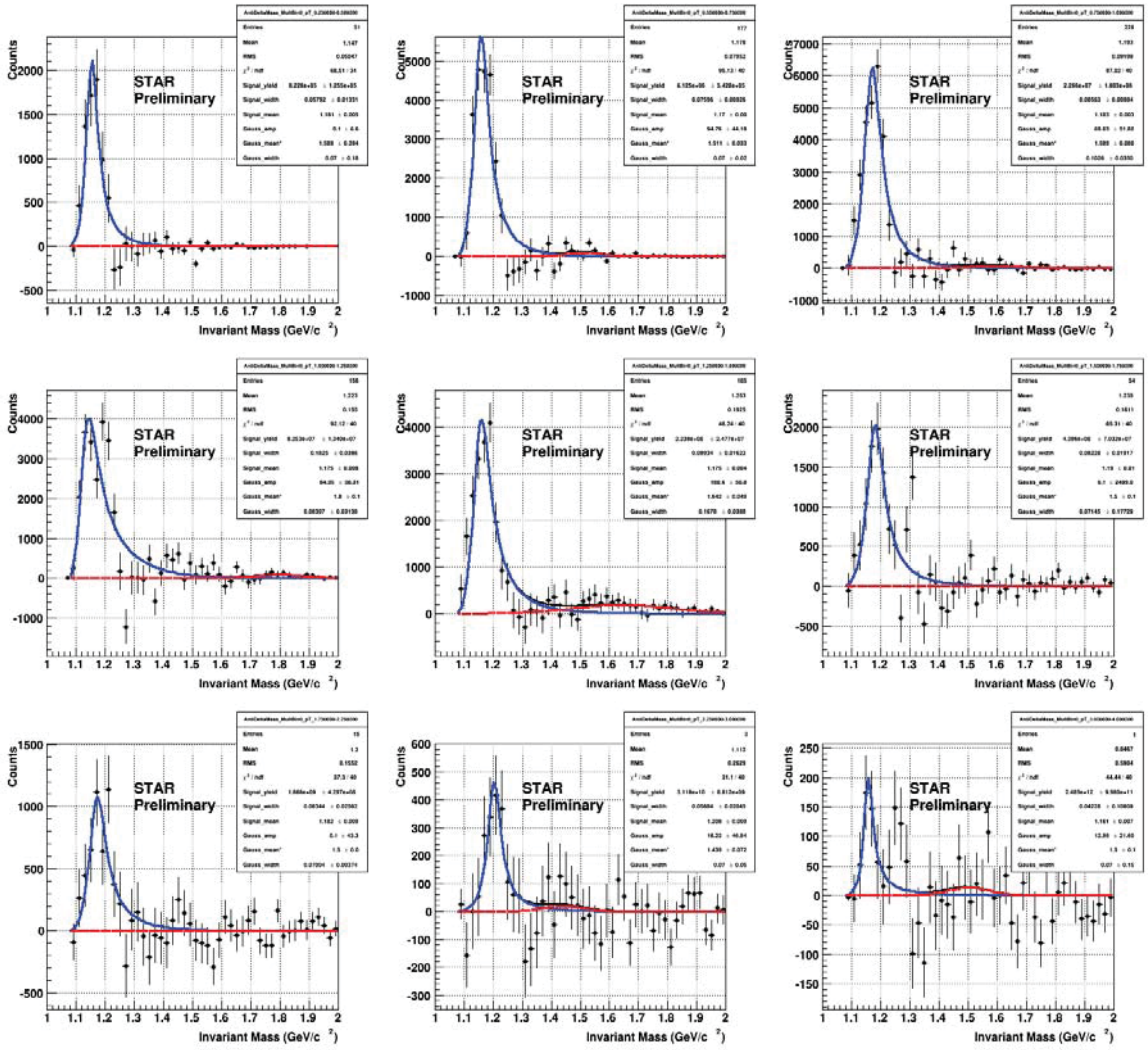

Figure 16: Shown are the relativistic Breit-Wigner fits of the $\overline{\Delta}$ invariant mass distribution for 50%-60% centrality. The $\overline{\Delta}$ signal was obtained using the rotation method. The centrality bin is divided into 9 p_T bins. Lowest to highest p_T appear left to right then top to bottom. The solid blue line fits the signal, while the red line is the Gaussian function that is used to account for any residual background.

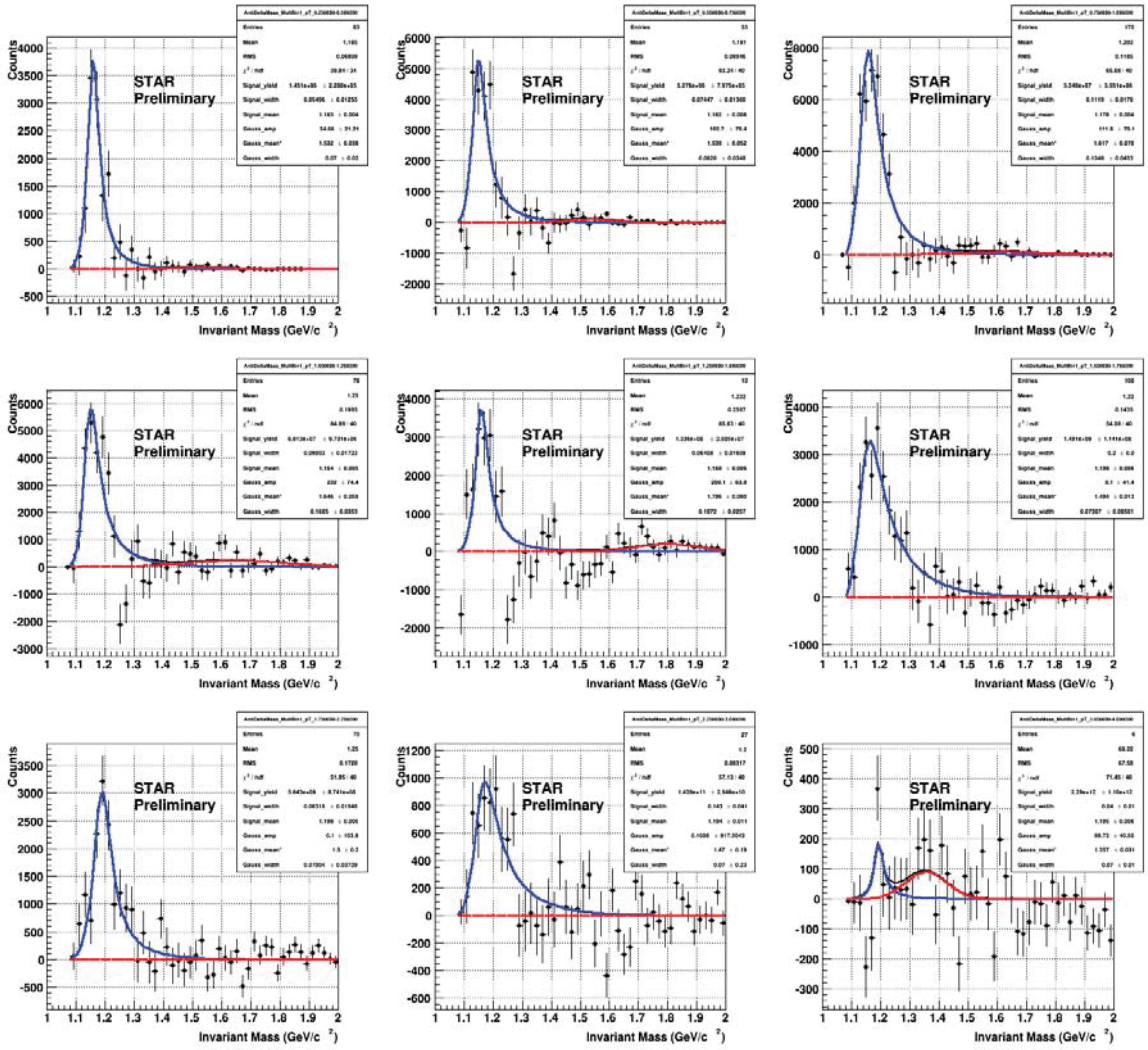

Figure 17: Shown are the relativistic Breit-Wigner fits of the $\overline{\Delta}$ invariant mass distribution for 40%-50% centrality. The $\overline{\Delta}$ signal was obtained using the rotation method. The centrality bin is divided into 9 p_T bins. Lowest to highest p_T appear left to right then top to bottom. The solid blue line fits the signal, while the red line is the Gaussian function that is used to account for any residual background.

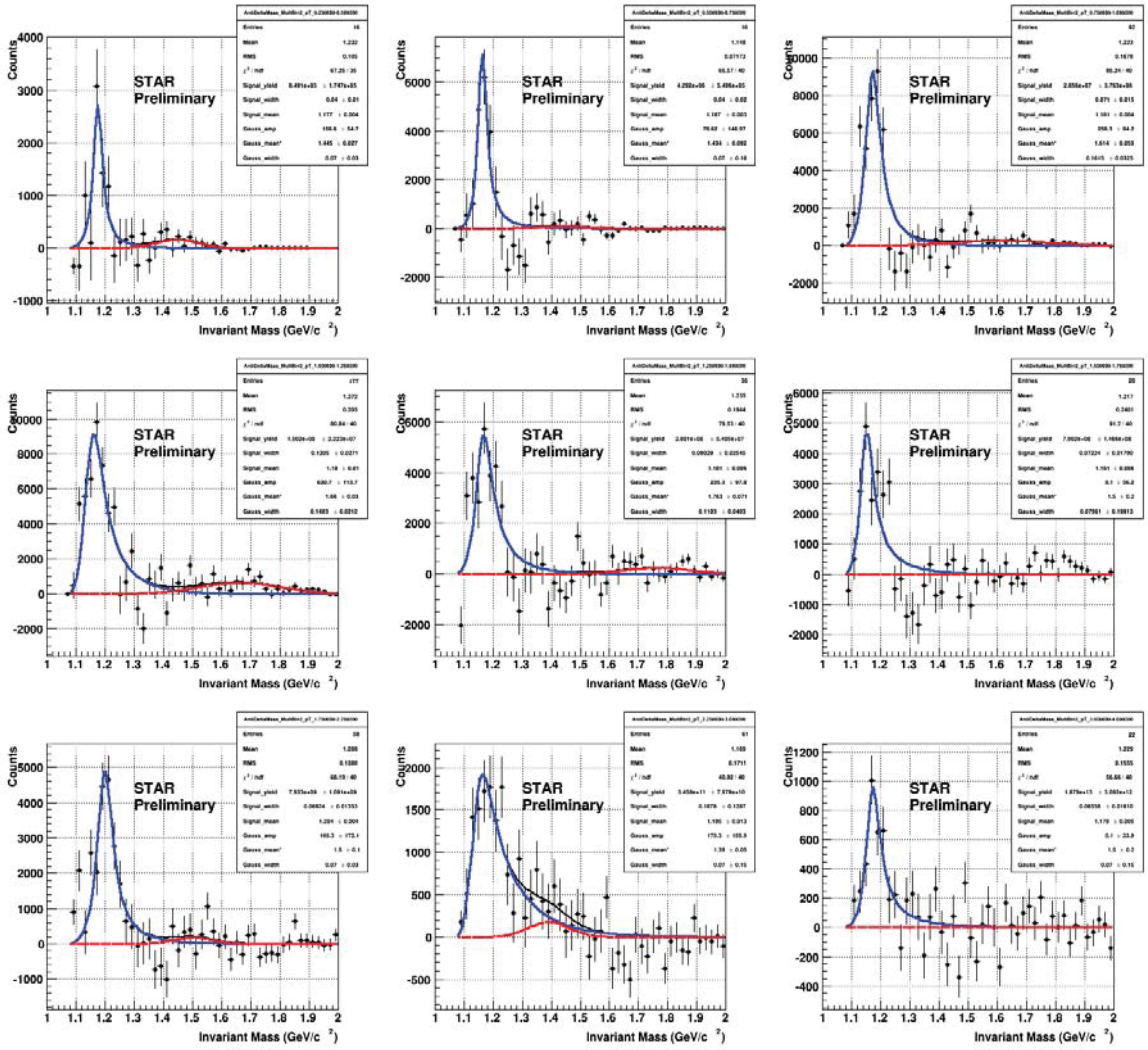

Figure 18: Shown are the relativistic Breit-Wigner fits of the $\overline{\Delta}$ invariant mass distribution for 30%-40% centrality. The $\overline{\Delta}$ signal was obtained using the rotation method. The centrality bin is divided into 9 p_T bins. Lowest to highest p_T appear left to right then top to bottom. The solid blue line fits the signal, while the red line is the Gaussian function that is used to account for any residual background.

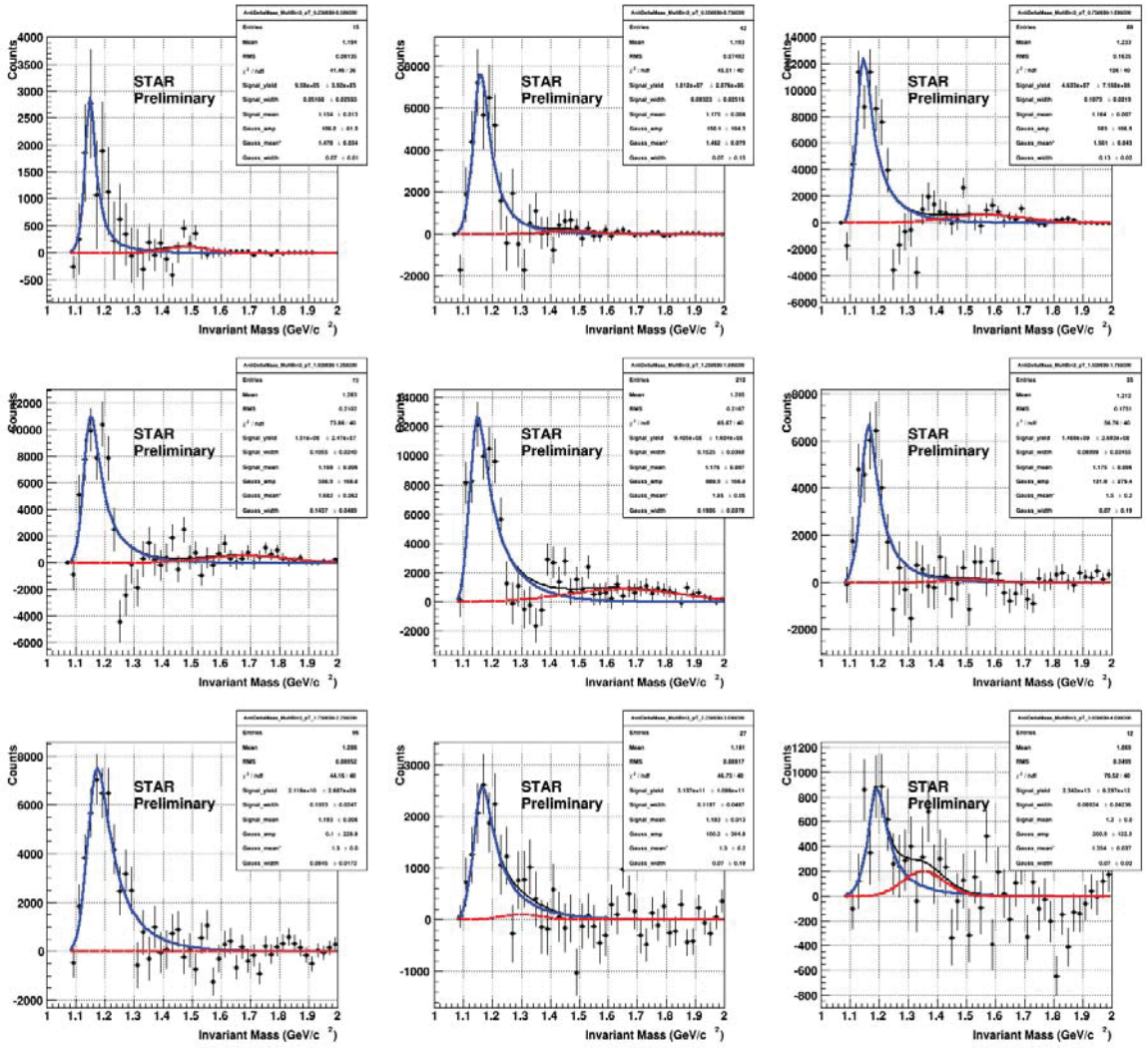

Figure 19: Shown are the relativistic Breit-Wigner fits of the $\overline{\Delta}$ invariant mass distribution for 20%-30% centrality. The $\overline{\Delta}$ signal was obtained using the rotation method. The centrality bin is divided into 9 p_T bins. Lowest to highest p_T appear left to right then top to bottom. The solid blue line fits the signal, while the red line is the Gaussian function that is used to account for any residual background.

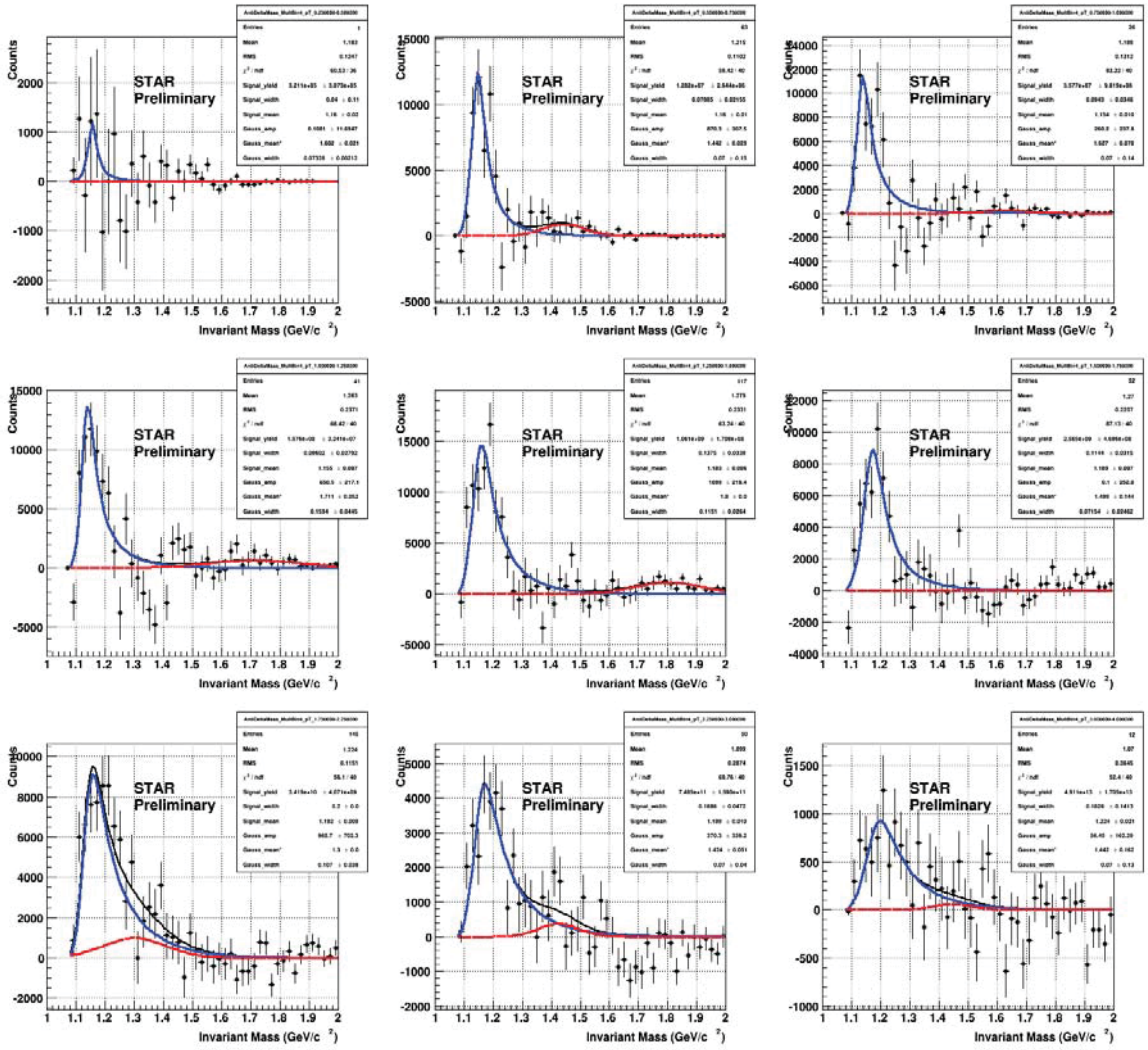

Figure 20: Shown are the relativistic Breit-Wigner fits of the $\overline{\Delta}$ invariant mass distribution for 10%-20% centrality. The $\overline{\Delta}$ signal was obtained using the rotation method. The centrality bin is divided into 9 p_T bins. Lowest to highest p_T appear left to right then top to bottom. The solid blue line fits the signal, while the red line is the Gaussian function that is used to account for any residual background.

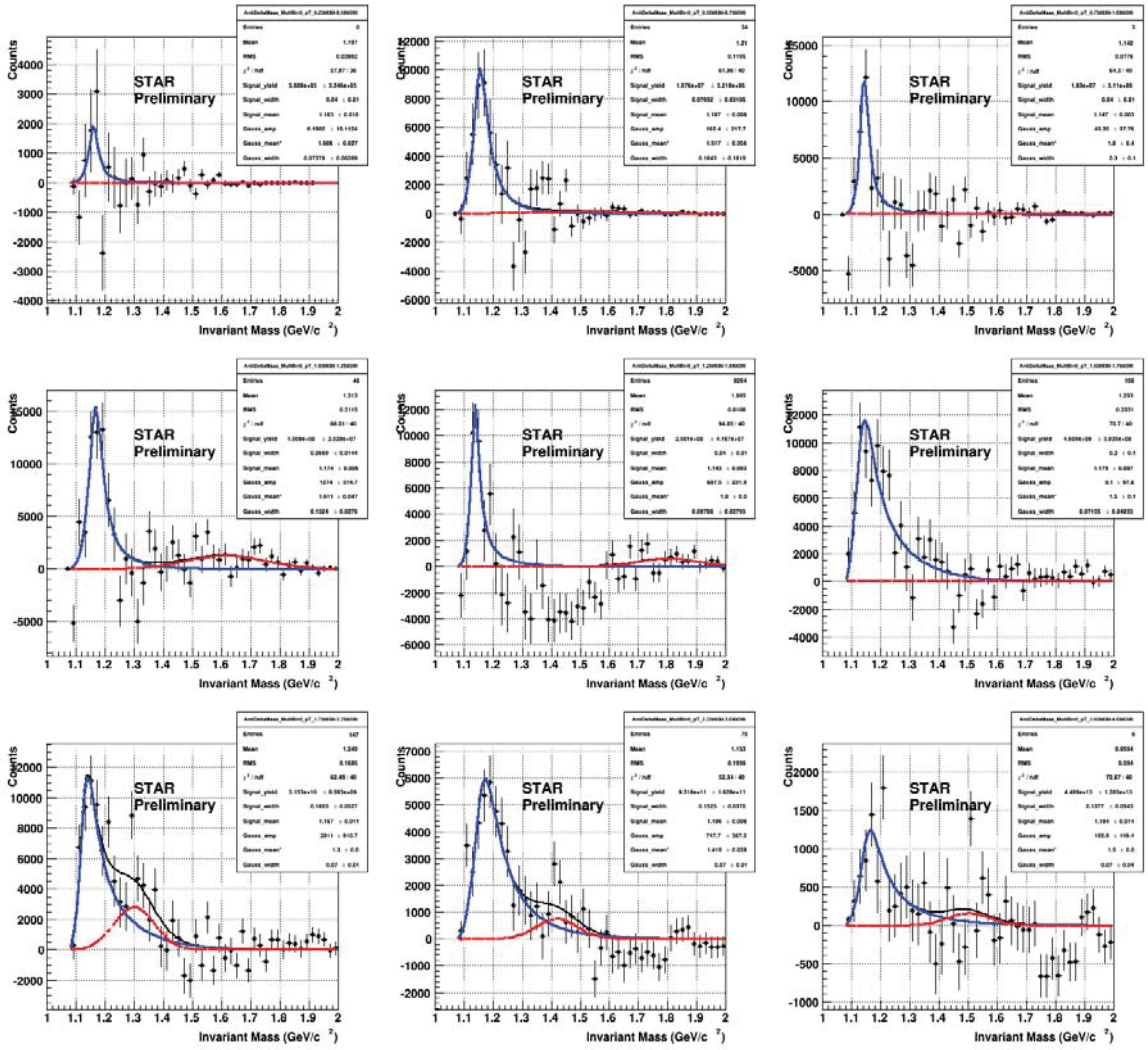

Figure 21: Shown are the relativistic Breit-Wigner fits of the $\overline{\Delta}$ invariant mass distribution for 0%-10% centrality. The $\overline{\Delta}$ signal was obtained using the rotation method. The centrality bin is divided into 9 p_T bins. Lowest to highest p_T appear left to right then top to bottom. The solid blue line fits the signal, while the red line is the Gaussian function that is used to account for any residual background.

mass shift of about 50 MeV/c^2 below the accepted value of 1232 MeV/c^2. The mass shift for 200 GeV proton-proton collisions and 200 GeV deuteron-gold collisions reported by STAR in 2008 was also about 50 MeV/c^2[18]. Due to these results, it does not appear that the mass shift is dependent on the size of the collision system. The mass shift is nearly constant within systematic error and uncertainty for all six centrality bins and across the measured p_T range. For this reason, it does not appear that the mass shift is dependent on centrality or p_T. To highlight this, the Δ masses for all six centrality bins are shown on a single plot in Figure 23, the average Δ mass is determined to be 1178 $\pm$ 1 MeV/c^2. The same is done for the $\overline{\Delta}$ masses in Figure 24, the average $\overline{\Delta}$ mass is determined to be 1173 $\pm$ 1 MeV/c^2.

Figure 25 shows the Δ and $\overline{\Delta}$ Breit-Wigner widths determined in our analysis of 200 GeV Cu+Cu collisions. For comparison between centrality bins, the Δ widths are shown on a single plot in Figure 26, the average Δ width is determined to be 85 $\pm$ 2 MeV/c^2. The same is done for the $\overline{\Delta}$ widths in Figure 27, the average $\overline{\Delta}$ width is determined to be 64 $\pm$ 2 MeV/c^2. We cannot conclude that there is any modification of the delta width due to the current level of uncertainties. The smallest systematic error for the width values, determined by comparing the different methods of background subtraction, is about 50 MeV/c^2. The results for 200 GeV proton-proton collisions and 200 GeV deuteron-gold collisions reported by STAR in 2008 also did not find any delta width modifications [18].

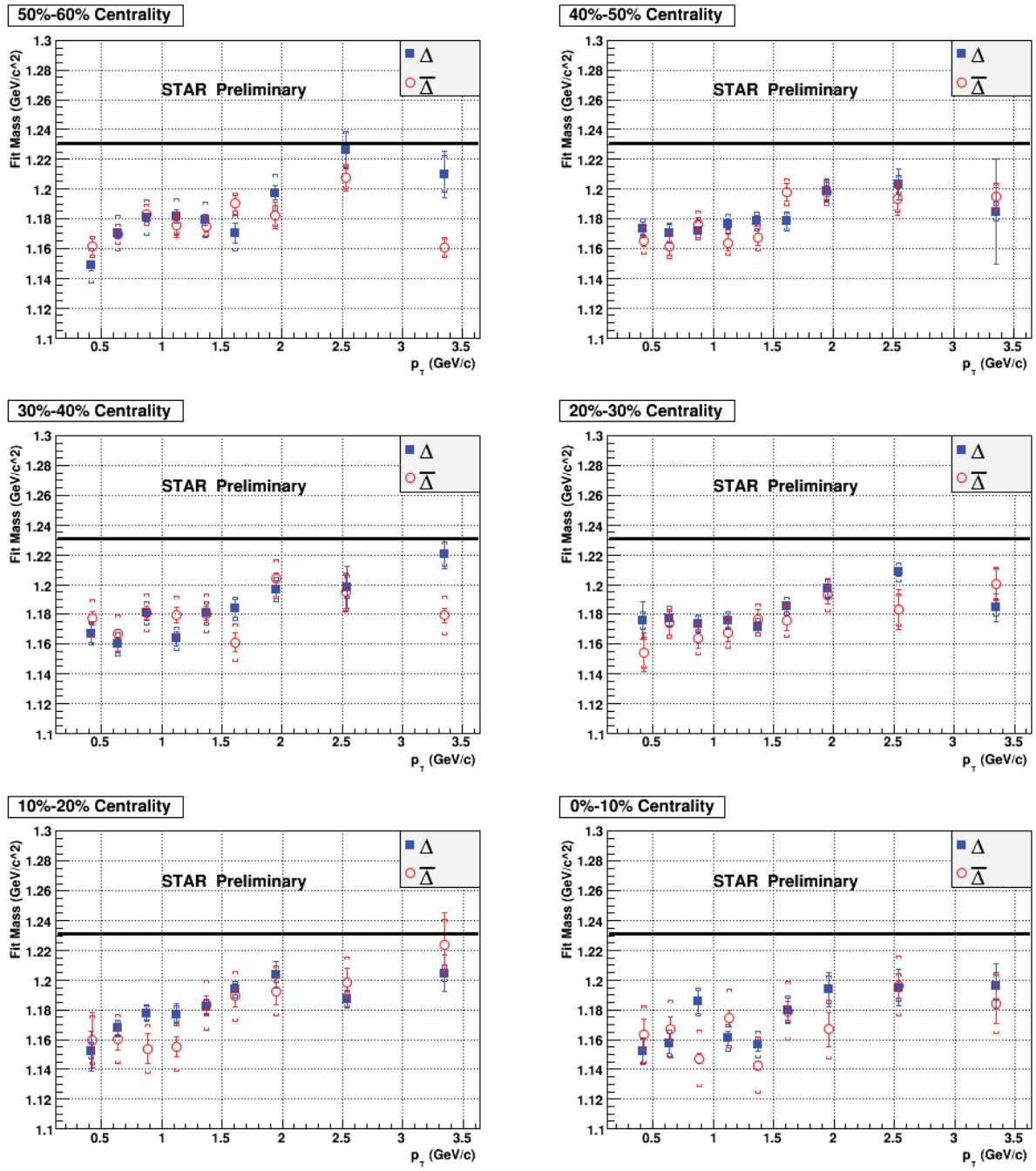

Figure 22: Shown are the Δ and $\overline{\Delta}$ mean mass values extracted from the relativistic Breit-Wigner fits. The mass values are divided in six centrality bins. The vertical axis for each plot is the mean mass value and the horizontal axis is p_T. The accepted mean mass of 1232 MeV/c^2 is marked as a solid black line. The brackets are the estimated systematic error for this analysis and the error bars are the uncertainties of the fit parameters.

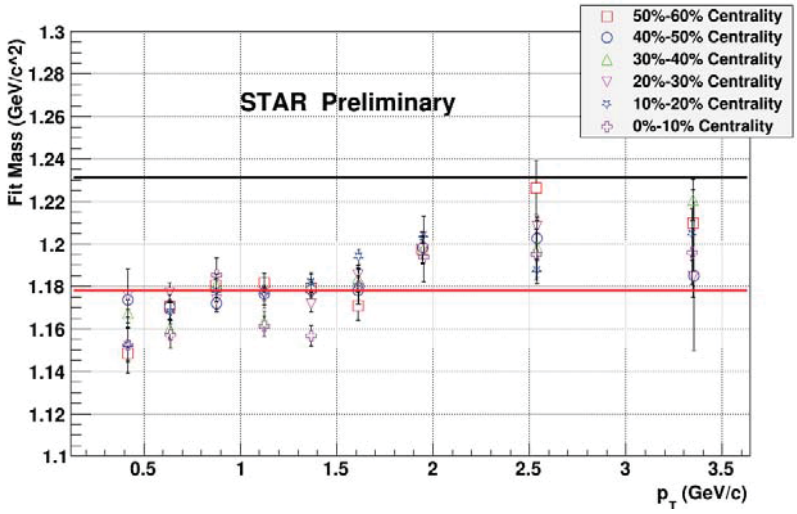

Figure 23: Shown are the Δ mean mass values for all six centrality bins on the same plot. The vertical axis is the mean mass value and the horizontal axis is p_T. The accepted mean mass of 1232 MeV/c^2 is marked as a solid black line. The average mean mass of 1178 MeV/c^2 is marked as a solid red line. The error bars are the uncertainties of the fit parameters.

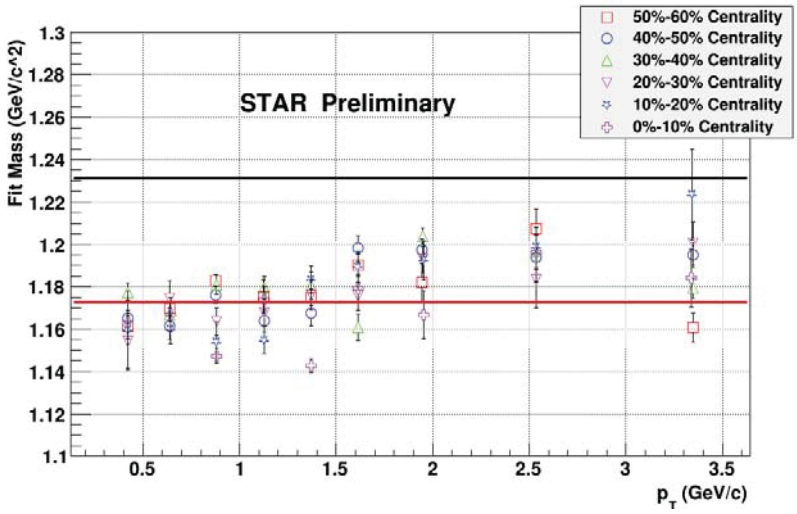

Figure 24: Shown are the $\overline{\Delta}$ mean mass values for all six centrality bins on the same plot. The vertical axis is the mean mass value and the horizontal axis is p_T. The accepted mean mass of 1232 MeV/c^2 is marked as a solid black line. The average mean mass of 1173 MeV/c^2 is marked as a solid red line. The error bars are the uncertainties of the fit parameters.

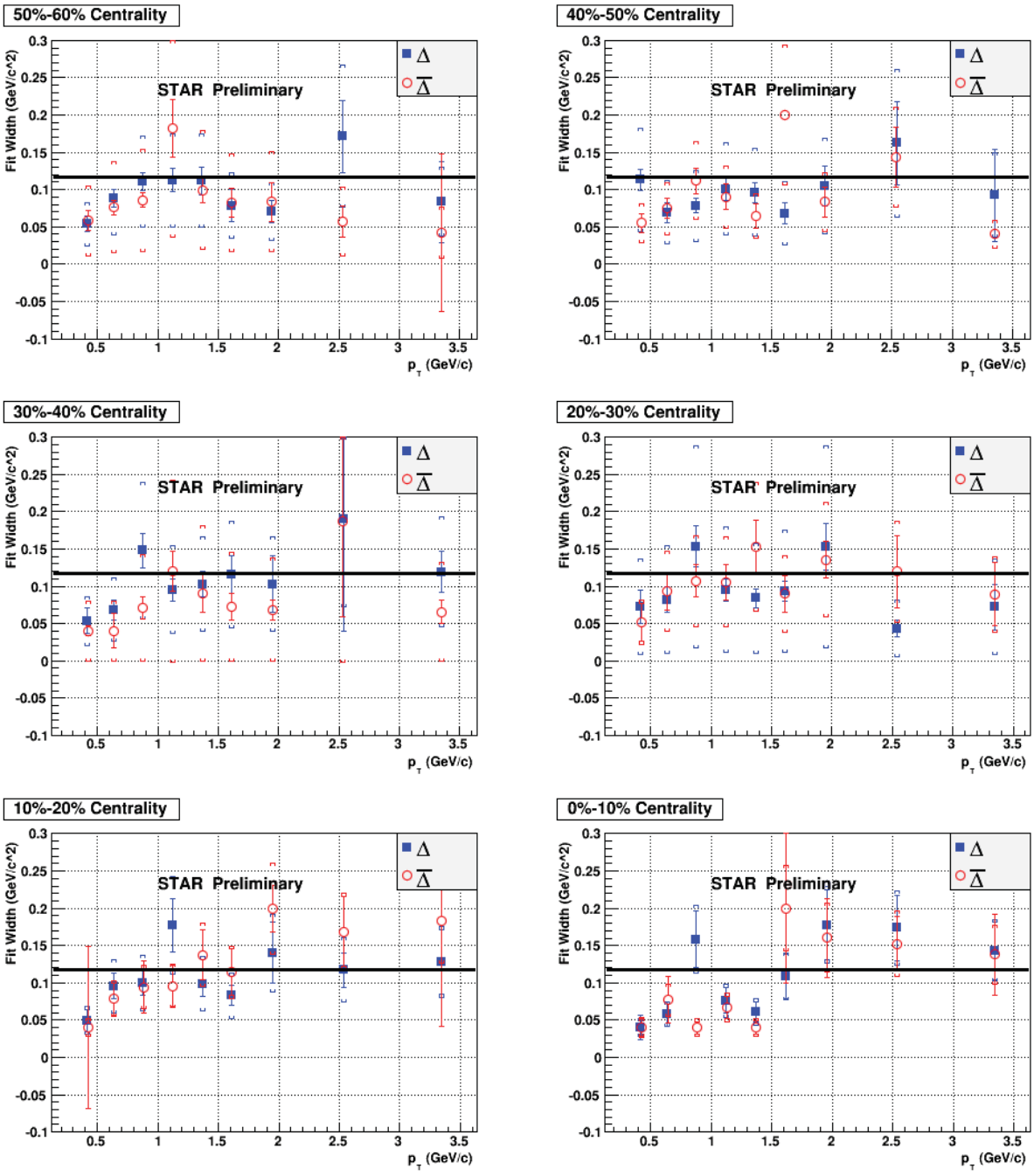

Figure 25: Shown are the Δ and $\overline{\Delta}$ Breit-Wigner width values in six centrality bins. The vertical axis for each plot is the width value and the horizontal axis is p_T. The accepted width of 117 MeV/c^2 is marked as a solid black line. The brackets are the estimated systematic error for this analysis and the error bars are the uncertainties of the fit parameters.

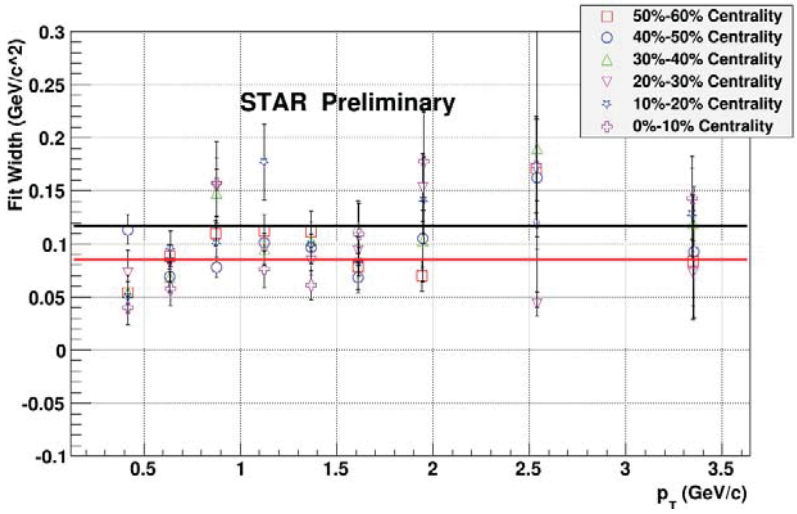

Figure 26: Shown are the Δ Breit-Wigner width values for all six centrality bins shown on the same plot. The vertical axis is the width value and the horizontal axis is p_T. The accepted width of 117 MeV/c^2 is marked as a solid black line. The average width of 85 MeV/c^2 is marked as a solid red line. The error bars are the uncertainties of the fit parameters.

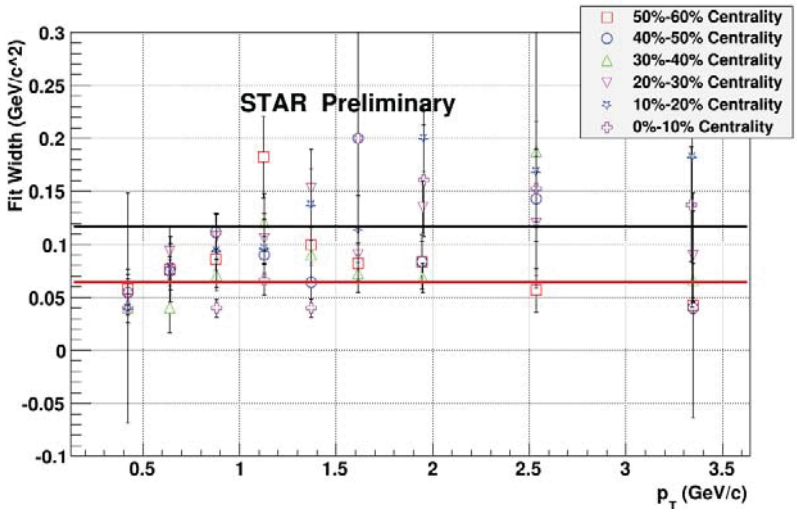

Figure 27: Shown are the $\overline{\Delta}$ Breit-Wigner width values for all six centrality bins shown on the same plot. The vertical axis is the width value and the horizontal axis is p_T. The accepted width of 117 MeV/c^2 is marked as a solid black line. The average width of 64 MeV/c^2 is marked as a solid red line. The error bars are the uncertainties of the fit parameters.

4.3 Yield Determination

To determine the yield of Δ's and $\overline{\Delta}$'s from each p_T bin, we integrated the relativistic Breit-Wigner fits shown in Figures 10-21. However, due to fluctuations of the width values for the Δ mass peaks, the yield values fluctuated as well. To reduce the fluctuations and to better determine systematic uncertainties, we switched to bin counting instead of integrating the fits. Bin counting means that we add the counts within all the individual histogram bins under each mass peak. We used the fit mean mass within each p_T bin to determine the center of the peak. We then included the bins within 55 MeV/c^2 on each side of the center of the peak in our determination of the yield of Δ's for that bin. 55 MeV/c^2 is slightly less than half the accepted Δ Breit-Wigner width. We used the higher mass region to the right of the Δ mass peaks to account for any residual background or over subtraction.

4.3.1 Acceptance and Efficiency Corrections

The bin counting method gives us the raw yield of Δ's measured in our analysis. These yield values must be corrected to account for the acceptance and efficiency of the TPC and STAR software. To determine what these corrections should be, we use a process known as "embedding." Embedding requires that we create simulated Δ's using a Monte Carlo generator, which are then flagged and placed into real 200 GeV Cu+Cu events at STAR. The embedded events are then run through STAR's software chain to determine if the daughter tracks of the simulated Δ's will be reconstructed. If the daughter tracks are able to be reconstructed, they are then subjected to the cuts used in our analysis, outlined in Table 2.

Only simulated Δ's within 55 MeV/c^2 of the 1232 MeV/c^2 Δ mass peak are considered to be successfully reconstructed. This is the same range used for our bin counting method and allows us to determine its efficiency. For each centrality and p_T bin, the number of simulated Δ's that pass cuts in our analysis is divided by the original number of Monte Carlo Δ's within the same bins. Only Monte Carlo Δ's within the same rapidity and primary vertex z range are used. The original Monte Carlo Δ's are not subjected to a mass range as the reconstructed Δ's are. This gives us the

Δ and $\overline{\Delta}$ acceptance and efficiency correction ratios shown in Figures 28 and 29. The original bin counting yields are corrected by dividing by these ratios. Then they are normalized to show the average yield of Δ's or $\overline{\Delta}$'s per event per unit rapidity at different p_T values. This is known as the transverse momentum spectra, or p_T spectra, and is shown in Figures 30 and 31.

Cut Description	**Accepted Values**
Primary Vertex Z (PVZ)	$\lvert$PVZ$\rvert < 50$ cm
Reference Multiplicity	> 19
N_{Hits} / $N_{HitsPossible}$	> 0.52
Track Rapidity	$\lvert$Rapidity$\rvert < 0.5$
Δ Decay Opening Angle	> 0.2 rad and < 1.8 rad
Δ Dip Angle	> 0.04 rad
Δ Daughter Momenta	$p_p > p_\pi$

Table 2: Events, Tracks, and Δ Candidates are required to pass these cuts during embedding. Particle identification cuts are not used.

4.3.2 Transverse Momentum Spectra Fits

To determine the total yield of Δ's from each centrality bin, we fit the p_T spectra with two different fit functions. The first function used to represent the Δ p_T spectra is known as a Boltzman function. It represents a thermal distribution and best represents the Δ p_T spectra at low p_T. The Boltzman function is given as

$$\frac{1}{2\pi p_T}\frac{d^2N}{dydp_T} = \frac{dN}{dy}\frac{\sqrt{p_T^2+m_0^2}}{2\pi T(m_0^2+2m_0T+2T^2)} \times \exp\left(\frac{-\left(\sqrt{p_T^2+m_0^2}-m_0\right)}{T}\right), \qquad (10)$$

where the term to the left of the equals sign is the normalized yield per unit rapidity (y) per unit p_T [21]. On the right of the equals sign, the term dN/dy is the normalized yield per unit rapidity for the centrality bin being fit. p_T remains transverse momentum, and m_0 is the accepted mean mass for the Δ. T is known as the inverse slope parameter and is historically related to the temperature of the medium. Within the Boltzman fits, dN/dy and T are treated as free parameters.

The second function used to represent the p_T spectra is known as a Levy function. The Levy function is similar to the Boltzman function at low p_T where it acts as an exponential function in order to represent the yield of Δ's produced by soft-scattering processes. However, at high p_T the

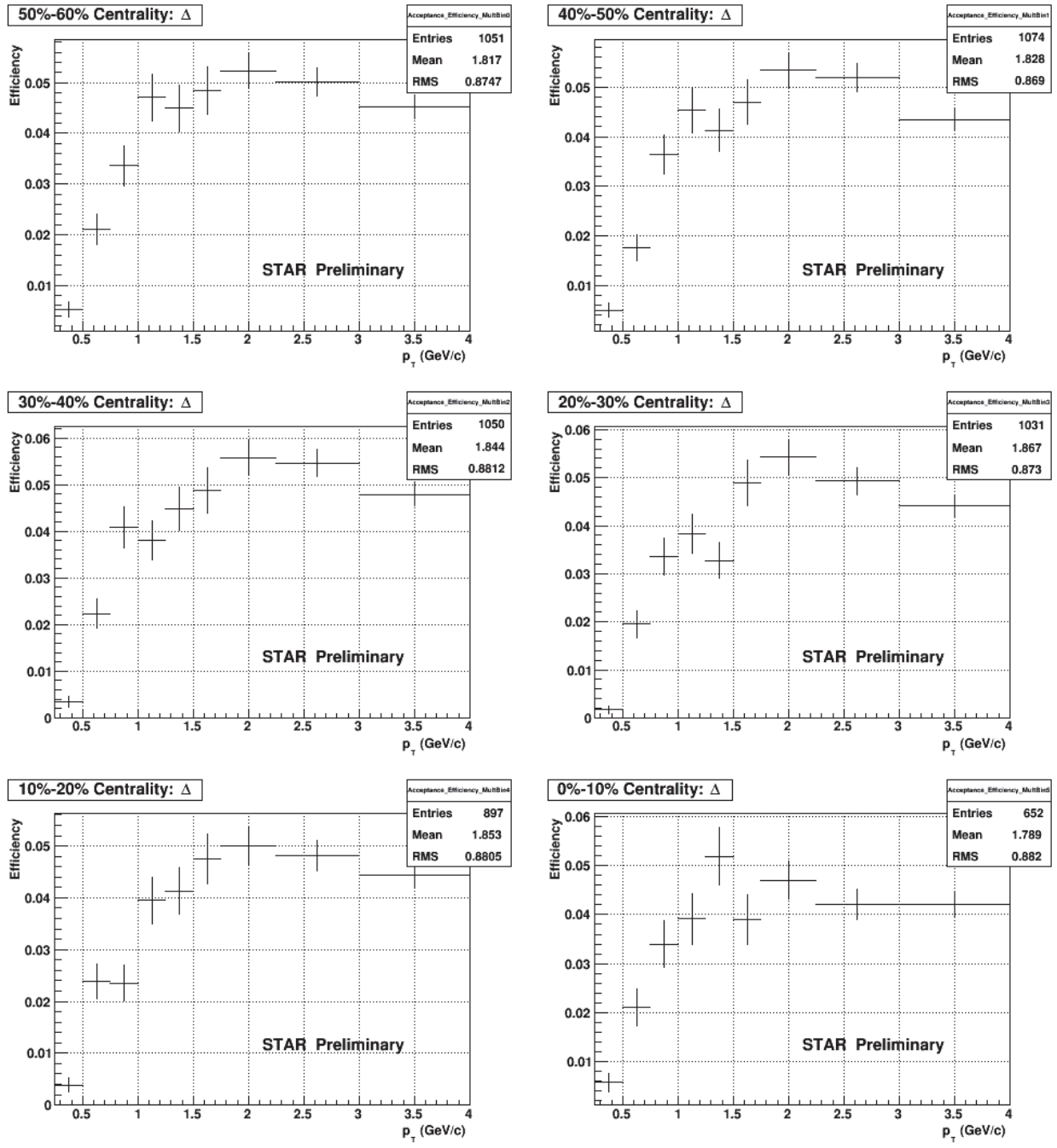

Figure 28: Shown are the Δ acceptance and efficiency correction ratios determined using embedding. The correction ratios are displayed on the y-axis as a function of p_T for each of the six centrality bins. The raw yields determined by the bin counting method are divided by these values to determine the actual yield of Δ's.

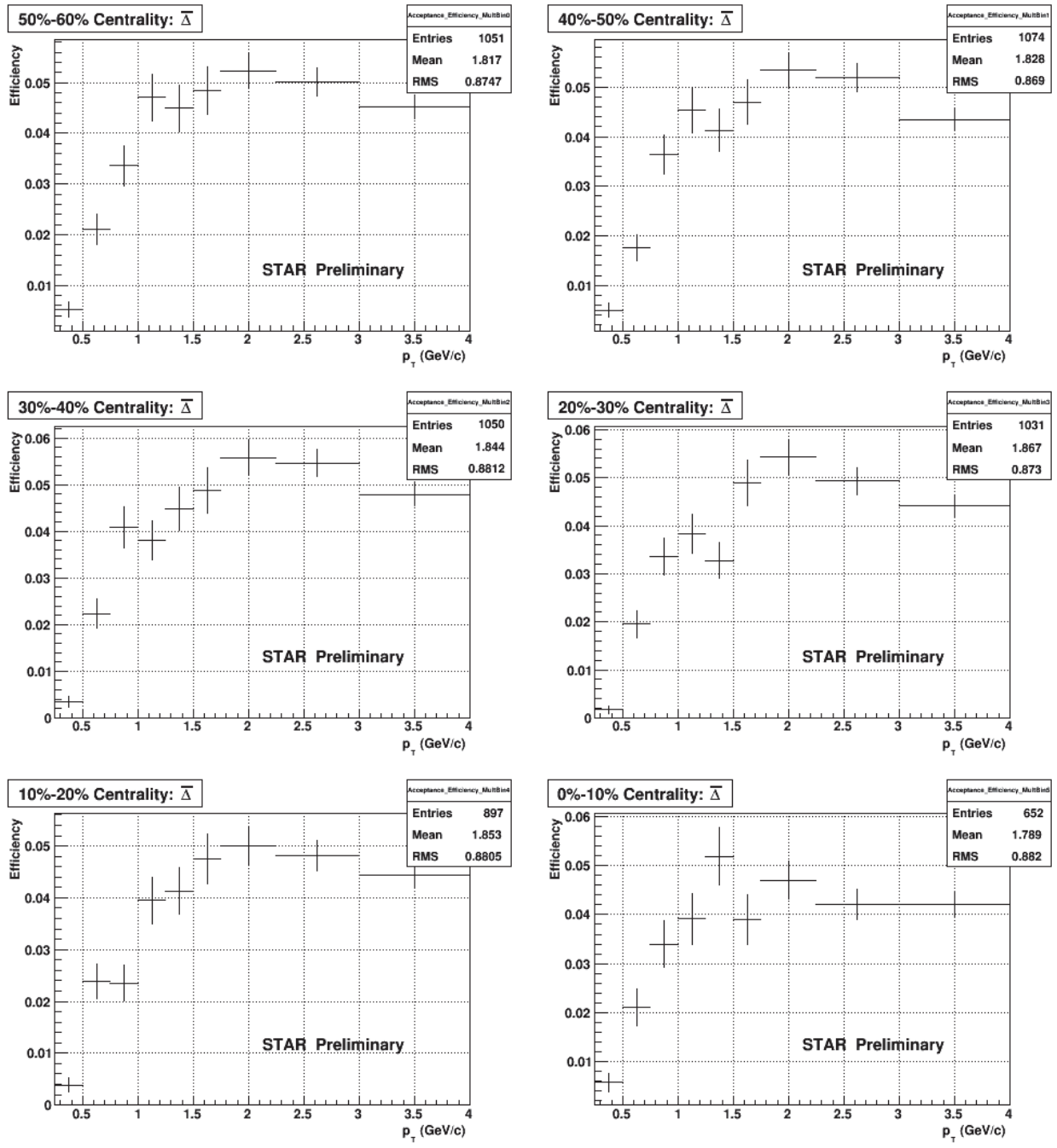

Figure 29: Shown are the $\overline{\Delta}$ acceptance and efficiency correction ratios determined using embedding. The correction ratios are displayed on the y-axis as a function of p_T for each of the six centrality bins. The raw yields determined by the bin counting method are divided by these values to determine the actual yield of $\overline{\Delta}$'s.

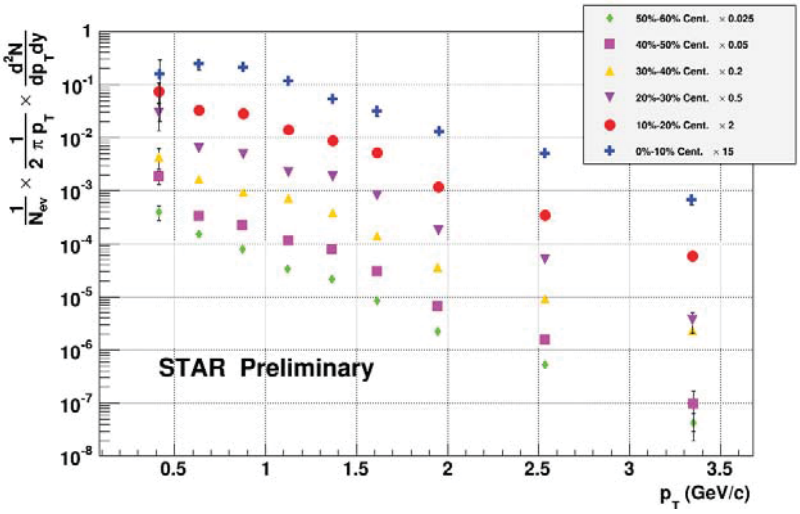

Figure 30: Shown is the corrected Δ p_T spectra for each centrality bin of the 200 GeV Cu+Cu collision system. The y-axis is the normalized Δ yield and the x-axis is p_T. All six centrality bins are multiplied by constants shown in the legend so that they appear neatly. Error bars indicate statistical uncertainties only.

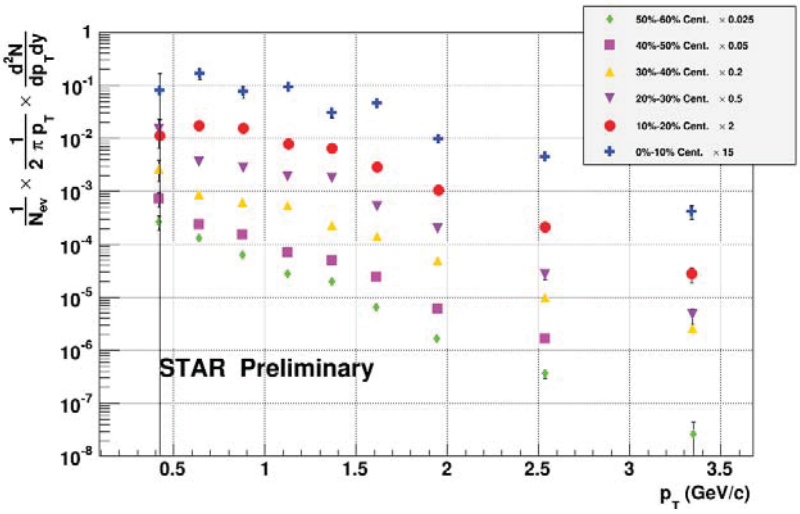

Figure 31: Shown is the corrected $\overline{\Delta}$ p_T spectra for each centrality bin of the 200 GeV Cu+Cu collision system. The y-axis is the normalized $\overline{\Delta}$ yield and the x-axis is p_T. All six centrality bins are multiplied by constants shown in the legend so that they appear neatly. Error bars indicate statistical uncertainties only.

Levy function acts as a power-law function to capture the yield of Δ's produced by hard-scattering interactions such as jets. The Boltzman function is unable to represent the hgih p_T range. The Levy function is given as

$$\frac{1}{2\pi p_T}\frac{d^2N}{dydp_T} = \frac{dN}{dy}\frac{(n-1)(n-2)}{2\pi nT[nT+m_0(n-2)]} \times \left(1+\frac{\sqrt{p_T^2+m_0^2}-m_0}{nT}\right)^{-n}, \qquad (11)$$

where n is the order of the power-law used to represent the high p_T Δ's [22]. The other terms have the same meaning as they do for the Boltzman function. Within the Levy fits, dN/dy, n, and T are all treated as free fit parameters. The Levy and Boltzman fits for the Δ and $\overline{\Delta}$ p_T spectra for all six centrality bins are shown in Figures 32 and 33.

The paramater dN/dy, taken from the Levy and Boltzman fits, gives us the total normalized Δ and $\overline{\Delta}$ yields per unit rapidity for each centrality bin. The Levy fits better represent the p_T spectra because they are able to account for the effects of hard-scattering interactions at high p_T. The dN/dy values taken from the Boltzman fits are used to estimate the systematic error. This is done by finding the percent difference between the Levy fit and Boltzamn fit dN/dy values in each p_T bin. The percent difference is then averaged for the centrality bin, and the averaged percent difference is applied to each point as the systematic error. The results of this analysis are shown in Figure 34, where the normalized mid-rapidity yield per unit rapidity (dN/dy) values from each centrality bin are compared to the number of participants (N_{part}). N_{part} for each centrality bin is taken from previous STAR publications [23, 24]. As shown in Figure 34, the yield of Δ's and $\overline{\Delta}$'s increases for more central collisions.

5 Conclusions

In the 2008 STAR publication, a possible explanation for the observed Δ mass shift was that the proton and pion daughters used to reconstruct the Δ's may be re-scattering resulting in a phase space distortion [18]. Our results do not agree with this argument because we observe the same 50 MeV/c^2 mass shift for 200 GeV Cu+Cu collisions as was observed for p+p collisions and d+Au collisions at the same energy. Due to the larger system size of Cu+Cu, we would expect to see a

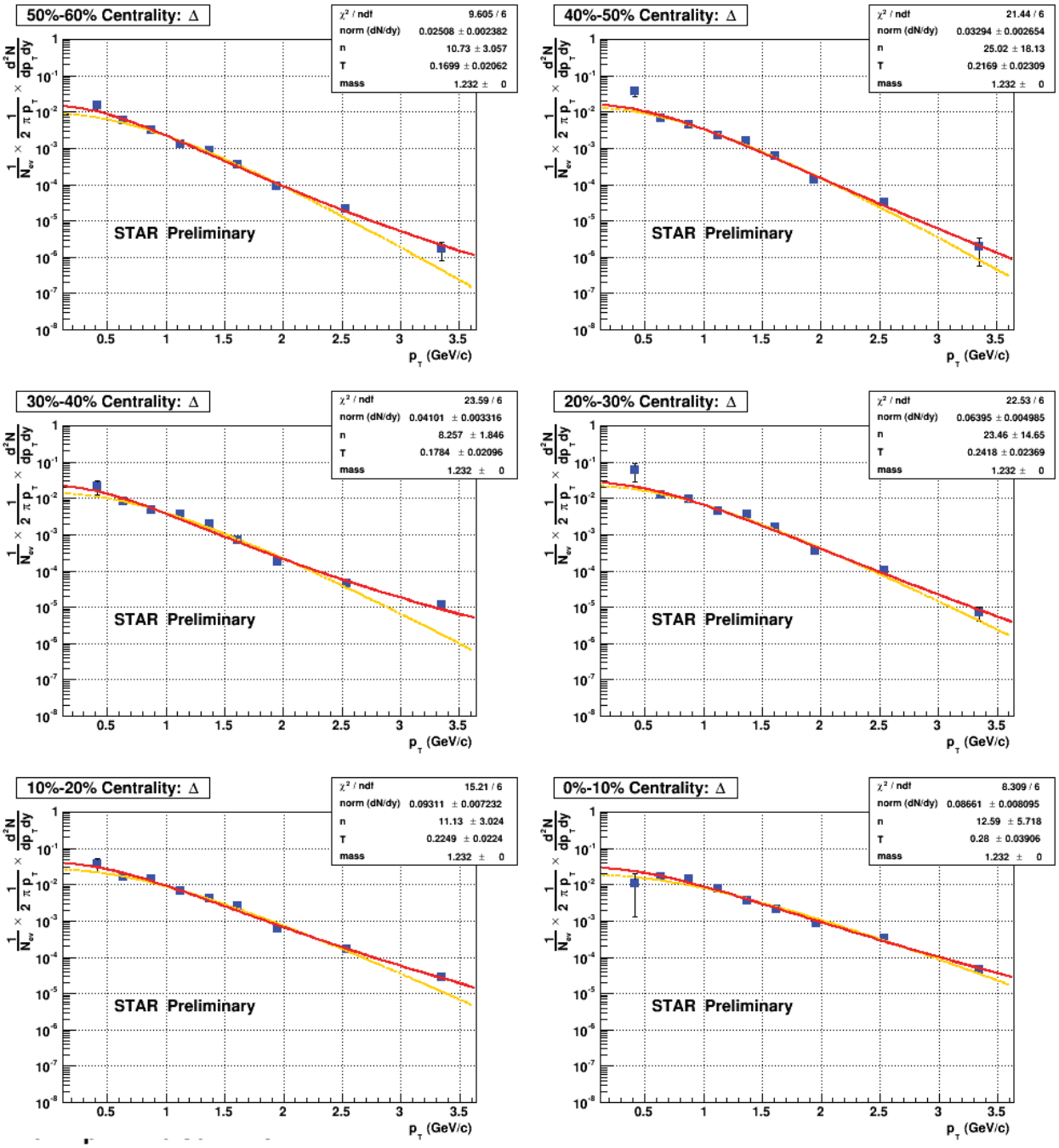

Figure 32: Shown are the Levy and Boltzman fits of the Δ p_T spectra for all six centrality bins. The y-axis of each plot is the normalized Δ yield per unit rapidity per unit p_T, and the x-axis is p_T. The Levy fits are shown as solid red lines, and the Boltzman fits are shown as dashed orange lines.

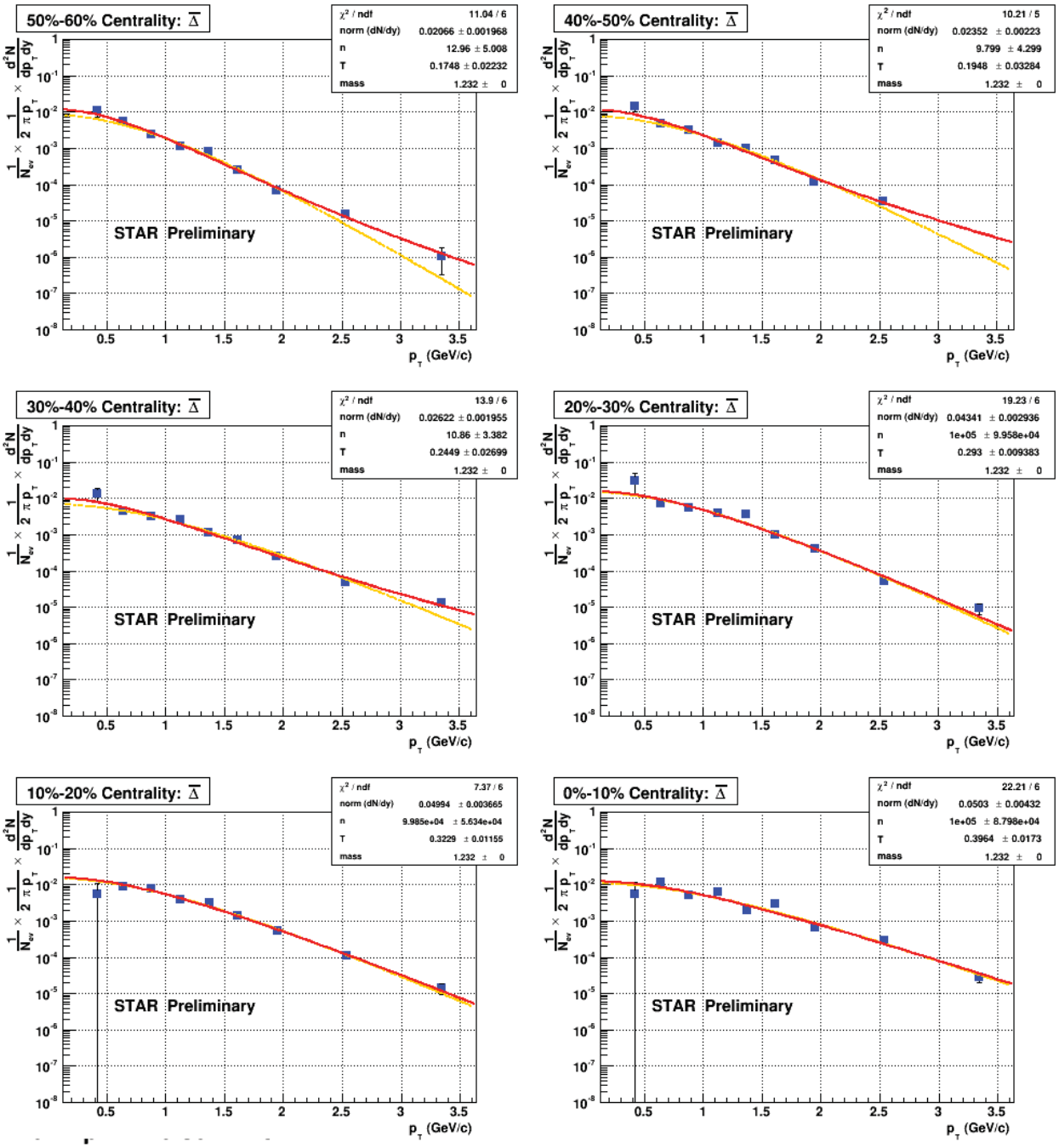

Figure 33: Shown are the Levy and Boltzman fits of the $\overline{\Delta}$ p_T spectra for all six centrality bins. The y-axis of each plot is the normalized $\overline{\Delta}$ yield per unit rapidity per unit p_T, and the x-axis is p_T. The Levy fits are shown as solid red lines, and the Boltzman fits are shown as dashed orange lines.

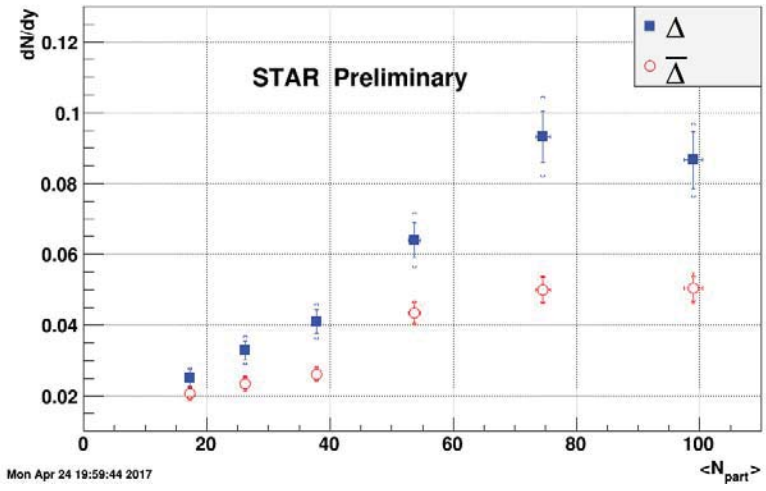

Figure 34: Shown are the Δ and $\overline{\Delta}$ mid-rapidity yields per unit rapidity for each centrality bin taken from the Levy fits. The systematic error is estimated by the difference in yield as determined by the Boltzman fits and Levy fits. We expect a larger contribution to the systematic error, perhaps as much as 10%-15%, from the difference between background subtraction methods (mixed events vs. rotation). The yield per unit rapidity is shown along the y-axis and the number of participants for each bin is shown along the x-axis. The Δ yields are shown as full blue squares, and the $\overline{\Delta}$ yields are shown as open red circles.

difference in the mass shift. The results of our analysis also showed that the mass shift is the same for both Δ's and $\overline{\Delta}$'s. In the 2008 STAR publication the Δ's and $\overline{\Delta}$'s were grouped together in order to improve statistics [18].

Within estimated error, the mass shift does not appear to be p_T dependent up to 3.5 GeV/c. This is complementry to the p+p and d+Au systems and extends the measured range in transverse momentum up to about 1.6 GeV/c. The observed mass shift is consistent within current uncertainties for all six centality bins, which range from 0% to 60% centrality. This result also does not agree with the phase space distortion explanation mentioned above. To understand what may be causing the mass shift a study of Δ's should be performed for lower energy collision systems. Perhaps the observed mass shift for the 200 GeV collision systems is an energy dependent effect.

The measured Δ and $\overline{\Delta}$ yields from our analysis will be useful for studying aspects of the 200 GeV Cu+Cu collision system. Currently we observe a rise in the mid-rapidity yields (dN/dy) that is dependent on collision centrality, shown in Figure 34. This is due to the increased net baryon

density at the primary vertex for more central collisions. We also observe that the ratio of Δ's to $\overline{\Delta}$'s is consistently greater than one. This is an expected result because antiquarks may only be produced by interactions during the collision, while the quarks that produce Δ's are already present in the nuclei.

The next step will be to compare these yields to the yields of stable particles such as protons and the yeilds predicted by theoretical models. As discussed earlier, a supression of Δ's may occur for higher centrality collisions depending on the lifetime of the medium. These results will reveal information about the time interval between chemical and kinetic freeze-out, and how this time interval depends on centrality. This information will be used by theorists to better understand the interactions taking place within heavy ion collisions.

Once the higher statistic results for Δ's and $\overline{\Delta}$'s produced in 200GeV p+p collisions are finalized by Dr. Witt, they can be compared to the 200 GeV Cu+Cu results produced in our analysis. This comparison will give us information about how the different centralities of Cu+Cu collisions compare to binary collisions within the p+p system. We will be able to scale the Δ and $\overline{\Delta}$ yields from the p+p collisions to match the number of binary collisions produced within each centrality bin using the Glauber Model. The Glauber Model is used to determine the number of binary collisions within heavy ion collisions at different centralities [25]. These results will allow us to determine the nuclear modification factor (R_{AA}) for Δ's and $\overline{\Delta}$'s produced by the 200 GeV Cu+Cu system. R_{AA} is a measurement of bulk matter effects within the Cu+Cu system and gives us more information about the production of QGP.

The measured Δ and $\overline{\Delta}$ yields will also be useful for other heavy ion physicists who need to account for the feed-down of protons and antiprotons from Δ and $\overline{\Delta}$ decays. My results provide the p_T spectra for Δ's and $\overline{\Delta}$'s up to 3.5 GeV/c for 0% to 60% centrality. Each Δ or $\overline{\Delta}$ is responsible for the production of a single proton or antiproton, so the feed-down of protons and antiprotons can be determined directly from our results.

References

[1] "RHIC Lessons," Accessed March 28, 2017, https://www.star.bnl.gov/lite/education/lessons.php.

[2] D. J. Gross and F. Wilczek, Phys. Rev. Lett. **30**, 1343 (1973); H. Politzer, Phys. Rev. Lett. **30**, 1346 (1973).

[3] D. Mishra, Ph. D. Dissertation, Study of Particle Multiplicity and Resonance Production at RHIC, (2005).

[4] "Supercomputing the Transition from Ordinary to Extraordinary Forms of Matter," Accessed November 28, 2016, https://www.bnl.gov/newsroom/news.php?a=24281.

[5] S. A. Bass, M. Belkacem, M. Bleicher, M. Brandstetter, L. Bravina, C. Ernst, L. Gerland, M. Hofmann, S. Hofmann, J. Konopka, G. Mao, L. Neise, S. Soff, C. Spieles, H. Weber, L. A. Winckelmann, H. Stocker, W. Greiner, Ch. Hartnack, J. Aichelin and N. Amelin, Prog. Part. Nucl. Phys. **41**, 225, (1998).

[6] "The UrQMD Model," Accessed April 20, 2017, http://urqmd.org/.

[7] "Recalling Quark Matter '83 and the Birth of RHIC," Accessed April 20, 2017, https://www.bnl.gov/rhic/news2/news.asp?a=6204&t=today.

[8] "Brookhaven National Labs Relativistic Heavy Ion Collider," Accessed December 12, 2015. https://www.bnl.gov/rhic/complex.asp.

[9] Nuc. Instr. Meth. A, **499**, 633 (2003).

[10] "Solenoidal Tracker at RHIC: Conceptual Design Report." Web Only. June 1st. 1992: http://drupal.star.bnl.gov/STAR/files/StarCDR.pdf.

[11] C. Nattrass, Ph. D. Dissertation, "System, energy, and flavor dependence of jets through di-hadron correlations in heavy ion collisions," 49, (2009).

[12] Nuc. Instr. Meth. A, **499**, 624 (2003).

[13] Nuc. Instr. Meth. A, **499**, 659 (2003).

[14] H. Bethe und J. Ashkin in "Experimental Nuclear Physics, ed. E. Segr, J. Wiley, New York, 1953, p. 253.

[15] EPJ Web Conf. **36**, 00010 (2012).

[16] B.I. Abelev et al. (STAR Collaboration), Phys. Rev. Lett. **97**, 132301, "Strange baryon resonance production in $\sqrt{s_{NN}}$ = 200 GeV p + p and Au + Au collisions," (2006).

[17] K.A. Olive et al. (Particle Data Group), Chin. Phys. C **38**, 090001 (2014).

[18] B. I. Abelev et al. (STAR Collaboration), Phys. Rev. Lett. **123**, 0450v2, "Hadronic resonance production in d+Au collisions at $\sqrt{s_{NN}}$ = 200 GeV at RHIC," (2008).

[19] S. Blyth, Ph. D. Dissertation, "Using the ϕ meson to probe the medium created in Au+Au collisions at RHIC," (2007) and references there in.

[20] D. M. Manley, Private Communication, January 2017.

[21] M. Lamont, Ph. D. Dissertation, "Neutral Strange Particle Production in Ultra-Relativistic Heavy Ion Collisions at $\sqrt{s_{NN}}$ = 130 GeV," (2002) and references there in.

[22] J. Adams et al. (STAR Collaboration), Phys. Rev. C **71**, 064902, "K(892)* resonance production in Au+Au and p + p collisions at $\sqrt{s_{NN}}$ = 200 GeV," (2005).

[23] G. Agakishiev et al. (STAR Collaboration), Phys. Rev. Lett. **108**, 072301, "Strangeness Enhancement in Cu+Cu and Au+Au Collisions at $\sqrt{s_{NN}}$ = 200 GeV," (2012).

[24] A. Timmins, Ph. D. Dissertation, "Neutral Strange Particle Production in Relativistic Cu+Cu Collisions at $\sqrt{s_{NN}}$ = 200 GeV," (2008) and references there in.

[25] Białłas, Bleszyński, and Czyz, Nucl. Phys. B **111**, 461 (1976).

A Glossary of Terms

Baryon: composite particle consisting of three quarks bound together by gluons: a type of hadron.

Centrality: the size of a heavy ion collision, determined by the number of nucleons that participate in the collision.

Chemical Freeze-out: time at which final particle ratios are determined within a heavy ion collision.

Combinatoric Background: mass distribution created by reconstructing parent particles from daughters that have no correlation to each other.

Confinement: a property of the strong nuclear force preventing partons from escaping their bonds within hadrons.

Daughter: a particle that is the product of a heavier particle decay.

Deconfinement: the process by which quarks are released at very high temperature and baryon density.

Fragmentation: the creation of hadrons when partons are pulled apart with enough energy or a single parton is forced out of a quark gluon plasma.

Global Track: a track within the TPC that does not include the primary vertex as a hit.

Gluon: a fundamental particle that mediates the strong nuclear force and binds quarks together within hadrons.

Hadron: a composite particle consisting of quarks and/or antiquarks bound together by gluons.

Hadronization: the process by which partons recombine to form hadrons.

Hard-scattering: initial parton-parton interactions of a heavy ion collision resulting in very high momentum tracks.

Invariant Mass: mass of a particle in its own rest frame.

Jet: spray of particles created by the fragmentation of a high momentum parton from a hard-scattering interaction.

Meson: composite particle consisting of a quark bound to an antiquark: a type of hadron.

Multiplicity: number of particles produced by a heavy ion collision.

Parent: a particle that decayed into lighter particles.

Participant: a nucleon involved during a heavy ion collision.

Parton: a fundamental particle responsible for the substructure of nucleons: includes quarks and gluons.

Primary Track: a track within the TPC that is projected to be within 3 cm of the primary vertex, and includes the primary vertex as a hit.

Primary Vertex: center point of a heavy ion collision.

Quark: a fundamental particle that composes all known composite particles (i.e. protons and neutrons). Quarks come in six flavors; up, down, strange, charm, top, and bottom.

Quark Gluon Plasma (QGP): state of matter where quarks and gluons are no longer confined within hadrons.

Reconstruction: using the energy and momenta of daughter particles to determine the energy and momentum of their parent.

Resonances: hadrons with extremely short lifetimes.

Soft-scattering: lower momentum parton-parton interactions that occur after the initial hard-scattering of a heavy ion collision.

Spectator: a nucleon not involved during a heavy ion collision.

Kinetic Freeze-out: time at which inelastic interactions cease within a heavy ion collision.

Transverse Momentum (p_T): momentum perpendicular to the heavy ion beam line.